CLM-R 46

CLM-R 46

United Kingdom Atomic Energy Authority

RESEARCH GROUP

Report

ELECTRIC FIELD DISSOCIATION OF H_2^+

H. WIND

Culham Laboratory,

Culham, Abingdon, Berkshire

1965

Available from H. M. Stationery Office

EIGHT SHILLINGS NET

U.D.C.
539.186.6 : 546.11

UNCLASSIFIED
(Approved for Sale)

CLM - R 46

ELECTRIC FIELD DISSOCIATION OF H_2^+

by

H. WIND

A B S T R A C T

When an electric field of sufficient strength is applied H_2^+ dissociates into $H^o + H^+$. The probability of this process is computed in part I. For intermediate steps the electronic energy in the field of two coulomb-centres and the energy levels of H_2^+ are also derived. Both these were already known but not with sufficient accuracy for application in the present work.

In part II, two methods are described which were used to observe field dissociation.

The new data resulting from these are (1) There is a threshold electric field. This confirms the theory that H_2^+ has a finite number of states. (2) It is possible to detect individual levels. (3) It is possible to estimate the population of these levels.

The agreement between theory and experiment is good.

U.K.A.E.A. Research Group,
Culham Laboratory,
Nr. Abingdon,
Berks.

September 1965.

CONTENTS

PART I

1. INTRODUCTION

1.1 Applications of Field Dissociation

The production of a plasma by the injection of high energy (10 keV - 1 MeV) particles into a magnetic field is used in a large number of experiments at the present time in the field of plasma physics.

If the particle trajectories are determined by a constant external potential (e.g. a magnetic field), it follows from Liouville's theorem that the ion density in the magnetic trap cannot be higher than the maximum density attainable by focussing the beam without the presence of a magnetic trap. For a higher density to be obtained, an additional mechanism must intervene. Such a mechanism is the Lorentz ionization or dissociation process. When a particle moves in a magnetic field B with a velocity v, in a co-ordinate system moving with the particle, the particle sees an additional electric field $\vec{F} = \vec{v} \times \vec{B}$. This electric field can dissociate H_2^+ or ionize H^o. The Lorentz dissociation of H_2^+ is at the moment used in the DCX-1[1] magnetic mirror injection experiment.

The purpose of this investigation is to determine what fraction of an H_2^+ beam dissociates as a function of the electric field. This fraction depends on the population and position of highly excited vibrational levels.

1.2 Historical Background

In order to calculate the position of the energy levels a quantum-mechanical consideration of H_2^+ is necessary. In fact the calculation of the ground state energy of H_2^+ has played an interesting part in the development of the quantum theory.

In 1922, in the days of the old quantum theory, the energy of H_2^+ was known from experiments. It was derived from the energies required to ionize H^o and H_2 and the energy required to dissociate H_2. The energy of H_2^+ is made up of the energy, $\frac{1}{R}$, due to the Coulomb interactions of the two protons with one another, and the electron energy E, which is a rather more complicated function of R (this function is calculated in section 2.3).

The total energy has a minimum at about $R = 2$. In the old quantum theory, this minimum is the energy of H_2^+ in the ground state. (In the new quantum theory, the lowest vibrational level does not have zero energy and this energy has to be added.)

Niessen[2] and Pauli[3] calculated independently the electron trajectories for a double Coulomb centre; by applying Sommerfeld's quantization rule it turned out that there was a stable solution. However, the energy was found to be roughly double the known value. Unfortunately, at that time (1922) the reason for the discrepancy was thought to reside in the experiments rather than in the theory. After the publication of Schrodinger's new theory (1926), it was suggested that it be used to explain the discrepancy[4]. The first such attempt by Alexandrow[5] failed[6]. However, following a qulitative treatment by Hund[7], Burrau[8] calculated the correct energy of H_2^+. The accuracy of the results was improved subsequently by several authors[9],[10].

During 1953, Bates et al. gave the electron energy as a function of the internuclear separation R up to R = 9 (atomic units) in four significant figures[11].

1.3 Other Calculations of H_2^+ Energy Levels

The experimental observation of μ meson induced fusion in the hydrogen bubble chamber led to an increased interest in the three body system. Cohen[12] et al. using a variational method, calculated the energy up to R = 20 with an estimated error of 2×10^{-4}. Hiskes[13] used this energy to calculate the vibrational levels of H_2^+ for the field dissociation problem. He found that the highest level has a binding energy of 4×10^{-5} a.u. when vibrational as well as rotational energy is taken into account. The energy of the lowest level is 0.1 a.u. so that the error of 2×10^{-4} in the electron energy results in an error of $\frac{2 \times 10^{-4} \times 0.1}{4 \times 10^{-5}} = 50\%$ in the binding energy of the highest level. However the position of the highest level can be measured with an accuracy of better than 10% by measuring the minimum electric field required for dissociation. We have therefore calculated a more accurate value of the electron energy. Field dissociation provides an excellent test of the theory since an error of 10^{-5} in the energy results in an error of a few per cent in the value for the threshold field.

1.4 Advantage of Producing H_2^+ from H_3^+

H_2^+ is usually obtained by electron impact ionization of H_2, but Riviere and Sweetman observed that H_2^+ ions produced from the break-up of H_3^+ ions in a gas collision have a higher vibrational excitation than H_2^+ ions obtained direct from the source[14]. They suggested that this could be so since the separation of the protons in the ground state of the H_3^+ ions is about 3.6 atomic units, and this is considerably greater than the equilibrium separation of 2.0 a.u. for the H_2^+ ion. However this is still small compared with the mean separation of the highest excited state of H_2^+ which is about 18 a.u.

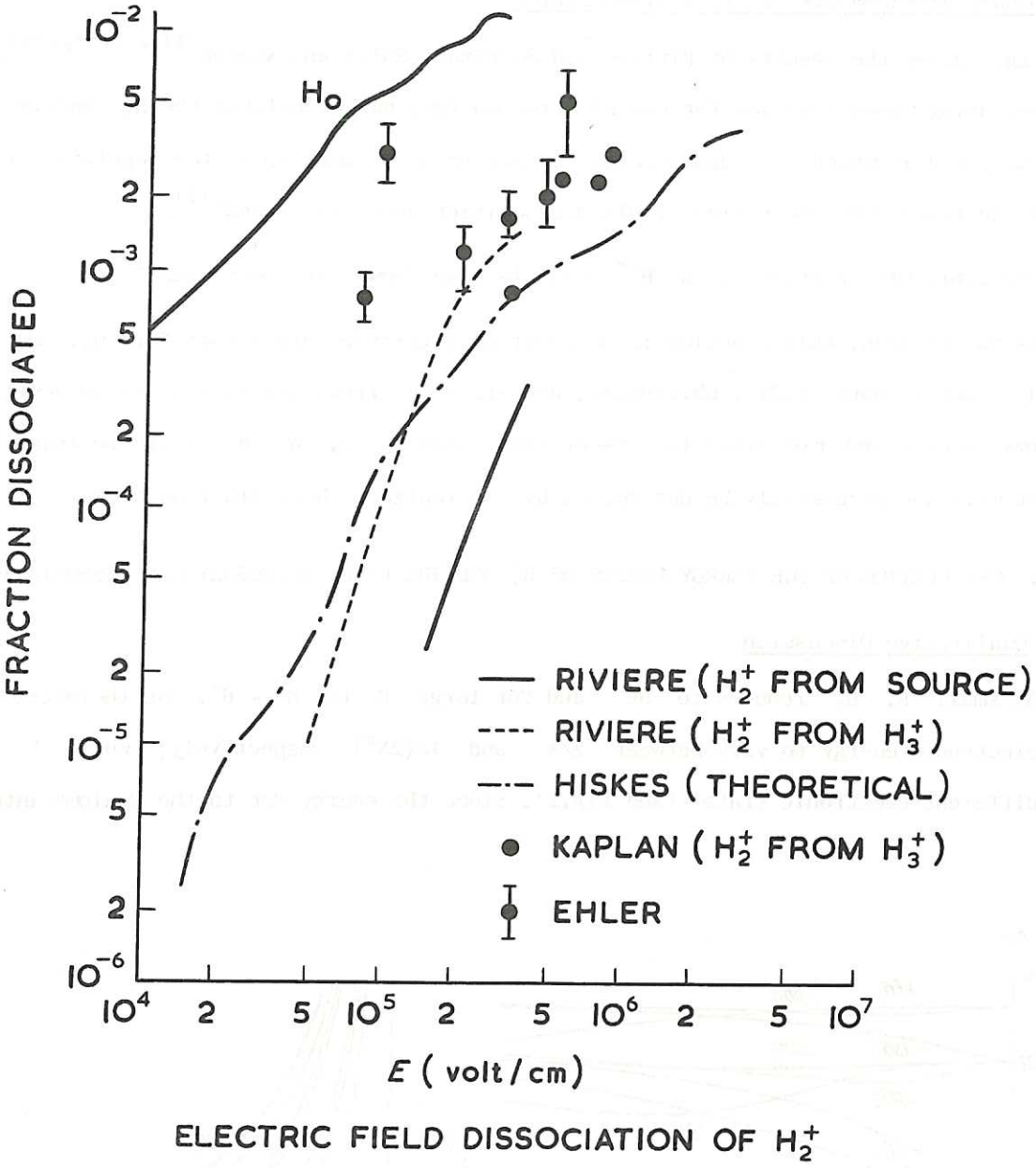

Fig. 1
The fraction of a H_2^+ beam dissociated as a function of the field applied

1.5 Other Measurements of Field Dissociation

Fig.1 gives the results of Riviere and Sweetman, Ehler and Kaplan[14], [15],[16]. Hiskes, using Cohen's values for the electron energy, has calculated the H_2^+ energy levels and the field at which they dissociate. By making an estimation of the population of these levels he found the theoretical field dissociation curve indicated[17].

The ionizable fraction of an H^{0*} beam is also shown for comparison[18].

As may be seen, this fraction is an order of magnitude larger than for H_2^+. However, an H_2^+ beam is more readily obtainable, and since the final ion density is in addition determined by a number of other factors of equal importance, the choice of the injection system will not necessarily be determined by the ionizable beam fraction alone.

2. CALCULATION OF THE ENERGY LEVELS OF H_2^+ AND THE FIELD NECESSARY FOR DISSOCIATION

2.1 Qualitative Discussion

At small R, H_2^+ reduces to He^+ and for large R to $H^0 + H^+$. We therefore expect the electronic energy to vary between $2/N^2$ and $1/(2N^2)$ respectively; where N labels the different electronic states (see Fig.2). Since the energy due to the Coulomb interaction

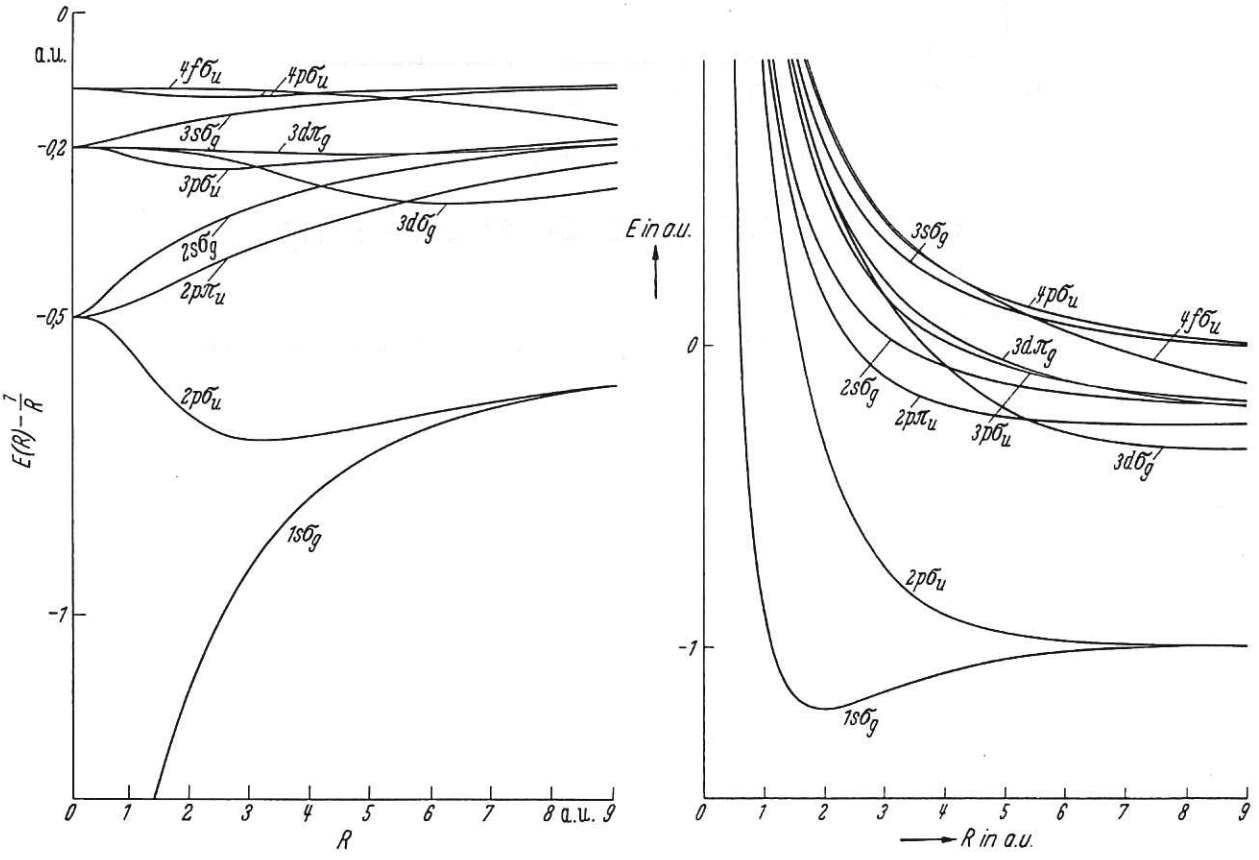

Fig. 2
The electron energies for two Coulomb-centres (left) and the sums of these electron energies and 1/R (right)

of the two protons, $1/R$, is to be added to the electronic energy to obtain the total energy, it can be expected that only the electronic ground-state is non repulsive. This is, however, not strictly true[11] since the $2p\sigma_u$, $3d\sigma_g$ and $2p\pi_u$ states have a shallow minimum. But because it is unlikely that these states are populated to a high extent, it is the electronic ground-state that is of the main interest for the present work.

Before starting the detailed calculation we can argue that for the electronic ground-state, there are a finite number of vibrational states.

We note that at large R, when H_2^+ is almost dissociated into H^o and H^+, the energy of the H^o, which is in the ground-state, is perturbed by the presence of H^+. The latter produces a field $1/R^2$ which according to the second order Stark effect varies the energy as $9/(4R^4)$. Considering the total potential we apply the Bohr-Sommerfeld quantization rule to estimate the quantum number of the top vibrational level.

$$nh = \int_{R_o}^{\infty} \sqrt{2[E - V(R)]M}\, dR$$

The fact that $E - V(R)$ approaches $9/(4R^4)$ for large R results in this integral being finite, which means that even for an energy equal to the dissociation energy, n is finite. We will see that the total number of vibrational states is 20.

2.2 The Wave Equation

We now calculate the electron energy and the vibrational and rotational levels. From these the field necessary for dissociation can be derived.

The Schrodinger equation for the H_2^+ ion is

$$\left\{ -\frac{\hbar^2}{2M}\left[\nabla_1^2 + \nabla_2^2\right] - \frac{\hbar^2}{2m}\nabla_e^2 + \frac{e^2}{4\pi\varepsilon|\vec{r}_1 - \vec{r}_2|} - \frac{e^2}{4\pi\varepsilon|\vec{r}_1 - \vec{r}_e|} - \frac{e^2}{4\pi\varepsilon|\vec{r}_2 - \vec{r}_e|} \right\} \varphi = E\varphi$$

Where the subscripts 1, 2 and e refer to the proton and electron co-ordinates respectively. M is the proton mass and m the electron mass.

From this the motion of the centre of gravity can be eliminated by the transformation.

$$\vec{R}_c = (M\vec{r}_1 + M\vec{r}_2 + m\vec{r}_e)/(2M + m)$$

$$\vec{R}_e = \vec{r}_e - \tfrac{1}{2}(\vec{r}_1 + \vec{r}_2)$$

$$\vec{R}_n = \vec{r}_1 - \vec{r}_2$$

The equation becomes

$$\left[-\frac{\hbar^2}{2}\left(\frac{1}{M_n}\nabla_n^2 + \frac{1}{M_e}\nabla_e^2\right) + \frac{e^2}{4\pi\varepsilon R_n} - \frac{e^2}{4\pi\varepsilon\left|\vec{R}_e - \tfrac{1}{2}\vec{R}_n\right|} - \frac{e^2}{4\pi\varepsilon\left|\vec{R}_e + \tfrac{1}{2}\vec{R}_n\right|}\right] \varphi\left(\vec{R}_e, \vec{R}_n\right) = W\varphi\left(\vec{R}_e, \vec{R}_n\right)$$

where $M_n = M/2$ and $M_e = m/(1 + m/2\,M)$

We have taken

$$M/m = 1836.096$$

The approximation now to be made originates from Born and Oppenheimer[19]. Messiah[20] explains this approximation as follows:

The mass of the electron is much smaller than the mass of the nuclei while the forces to which they are subjected are of comparable magnitude. As a consequence, the motion of the nuclei is very much slower than that of the electron, and, to a very good approximation, these two motions, electronic and nuclear, can be treated separately. Indeed in a first approximation the electron "sees" the nuclei as fixed force centers and the dynamical state is that of an electron circulating about fixed nuclei. Since the latter move slowly, the dynamical state of the electron adiabatically follows this gradual evolution in the potential to which it is subject. Conversely, since the electron describes many revolutions during any appreciable displacement of the nuclei, the latter are essentially subject to only the average effect. The motion of nuclei is obtained to a very good approximation by replacing their interaction with the electron by its average value over several electron revolutions. Application of this procedure leads to a Schrodinger equation in which the electron variable has completely disappeared. The approximation upon which this method of separation of variables is based is called the adiabatic approximation.

It is also called the Born-Oppenheimer approximation.

To apply this principle to our problem, a solution of the form

$$\varphi\left(\vec{R}_e, \vec{R}_n\right) = \psi\left(\vec{R}_e, \vec{R}_n\right)\chi\left(\vec{R}_n\right)$$

is introduced. The neglect of the effect of the nuclear motion on the electronic energy means that $\nabla_n\psi$ is neglected. The equation now becomes, after division by φ

$$-\frac{\hbar^2}{2M_n}\frac{\nabla_n^2\chi(\vec{R}_n)}{\chi(\vec{R}_n)} + \frac{e^2}{4\pi\varepsilon R_n} + -\frac{\hbar^2}{2M_e}\frac{\nabla_e^2\psi(\vec{R}_e, \vec{R}_n)}{\psi(\vec{R}_e, \vec{R}_n)} - \frac{e^2}{4\pi\varepsilon\left|\vec{R}_e - \tfrac{1}{2}\vec{R}_n\right|} - \frac{e^2}{4\pi\varepsilon\left|\vec{R}_e + \tfrac{1}{2}\vec{R}_n\right|} = W$$

Now $\frac{\hbar^2}{M_e}$ and $\frac{e^2}{4\pi\varepsilon}$ are introduced as unity. This means that the unit of energy is $\frac{M_e e^4}{(4\pi\varepsilon)^2\hbar^2}$ and the unit of length $\frac{\hbar^2 4\pi\varepsilon}{M_e e^2}$.

This leads to

$$-\frac{M_e}{2M_n}\frac{\nabla_n^2\chi(\vec{R}_n)}{\chi(\vec{R}_n)}+\frac{1}{R_n}+\left\{-\tfrac{1}{2}\frac{\nabla_e^2\psi(\vec{R}_e,\vec{R}_n)}{\psi(\vec{R}_e,\vec{R}_n)}-\frac{1}{|\vec{R}_e-\tfrac{1}{2}\vec{R}_n|}-\frac{1}{|\vec{R}_e+\tfrac{1}{2}\vec{R}_n|}\right\}=W$$

R_e appears now in the part in brackets only. This part is therefore independent of R_e. It represents the electron energy $E(R_n)$ for a fixed internuclear separation R_n. This will be solved in the next section.

A further simplification is possible by the substitution

$$\chi(\vec{R}_n)=\frac{\Pi(R_n)}{R_n}\,\Theta(\theta,\varphi)$$

where R_n, θ and φ are spherical co-ordinates.

This leads to

$$-\frac{M_e}{2M_n}R_n^2\frac{\nabla^2\Pi(R_n)}{\Pi(R_n)}+\left\{\frac{1}{R}+E(R_n)\right\}R_n^2=\frac{1}{\Theta(\theta,\varphi)}\left[\frac{1}{\sin\theta}\frac{\partial}{\partial\theta}\left(\sin\theta\frac{\partial\Theta}{\partial\theta}\right)+\frac{1}{\sin^2\theta}\frac{\partial^2\Theta}{\partial\varphi^2}\right]$$

The right hand side of this equation depends on θ and φ only and is therefore constant. The solution of this part is given by spherical harmonics:

$$\Theta(\theta,\varphi)=Y_{J,m}(\theta,\varphi)\ .$$

The constant value is $-J(J+1)$ which has a degeneracy of $2J+1$. The components are labelled $m=-J,\ldots.+J$ depending on the orientation. We will use the $Y_{J,m}$ functions in 2.5 for the probability distribution of the orientation with respect to an applied electric field.

The equation is now reduced to

$$\nabla^2\Pi(R_n)+\left\{\frac{2M_n}{M_e}\left[W-E(R_n)-\frac{1}{R_n}\right]-\frac{J(J+1)}{R_n^2}\right\}\Pi(R_n)=0$$

In Section 2.4 we will solve this equation. We will see that one more term is still to be added. This is the firstorder perturbation term from the Born-Oppenheimer approximation due to the motion of the nuclei.

2.3 The Electronic Energy. (Part of this has been published[21].)

The equation for the electronic energy expressed in confocal elliptic co-ordinates, λ and μ, and an azimuthal angle φ becomes[22]

$$\frac{\partial}{\partial\lambda}\left\{(\lambda^2-1)\frac{\partial\psi}{\partial\lambda}\right\}+\frac{\partial}{\partial\mu}\left\{(1-\mu^2)\frac{\partial\psi}{\partial\mu}\right\}+\left\{\frac{1}{\lambda^2-1}+\frac{1}{1-\mu^2}\right\}\frac{\partial^2\psi}{\partial\varphi^2}+\left\{\tfrac{1}{2}R^2E(\lambda^2-\mu^2)+2R\lambda\right\}\psi=0$$

(The subscript n on R_n is now deleted).

Writing $\psi(\lambda,\mu,\varphi) = \Lambda(\lambda)\, M(\mu)\Phi(\varphi)$ and $p^2 = -\frac{1}{2}R^2E$, the following equations are obtained,

$$\frac{d^2\Phi}{d\varphi^2} = -m^2\Phi \qquad \ldots (1)$$

$$\frac{d}{d\mu}\left\{(1-\mu^2)\frac{dM}{d\mu}\right\} + \left\{-A + p^2\mu^2 - \frac{m^2}{1-\mu^2}\right\}M = 0 \qquad \ldots (2)$$

$$\frac{d}{d\lambda}\left\{(\lambda^2-1)\frac{d\Lambda}{d\lambda}\right\} + \left\{A + 2R - p^2\lambda^2 - \frac{m^2}{\lambda^2-1}\right\}\Lambda = 0 \qquad \ldots (3)$$

where A is the separation constant. We will restrict ourselves to the case m = 0, (σ state)

(1) Gives immediately $\Phi(\varphi) = \exp(im\varphi) = 1$.

In (2) A is defined as a function of p by the additional condition that $M(\mu)$ shall be a proper function. By this is meant that both M and $\frac{dM}{d\mu}$ shall be continuous, single valued and finite. To examine which condition in this case is relevant, we have solved (2) by means of an analogue computer. In doing so A was varied around the correct value given by Bates[11]. When $\frac{dM}{d\mu}$ was plotted as a function of μ (see Fig.3) it was shown that the

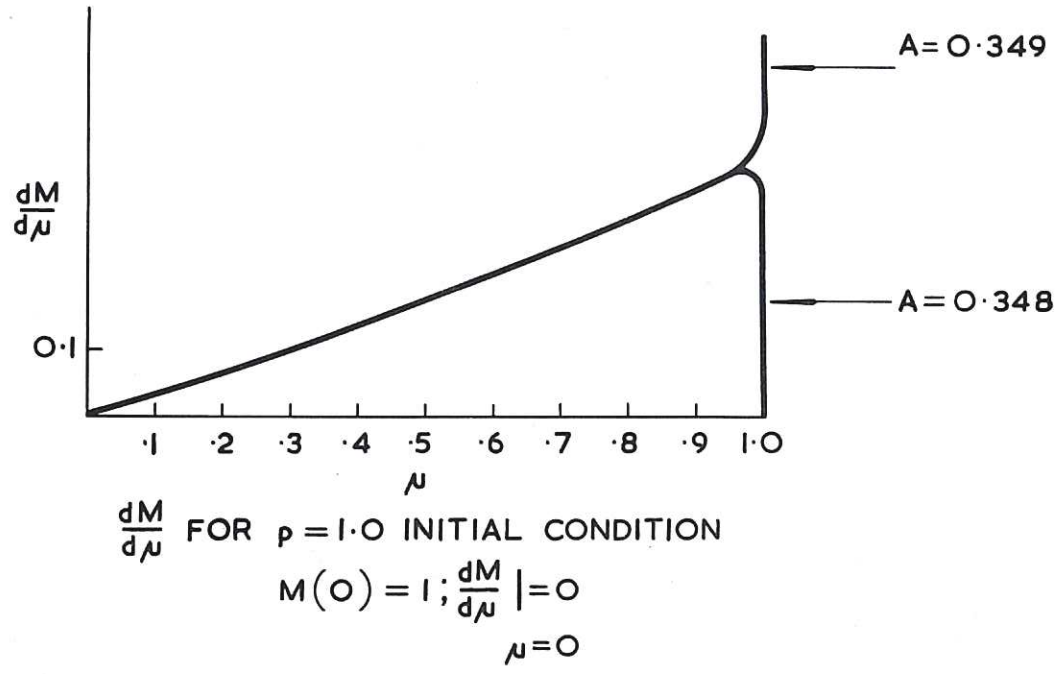

Fig. 3
The derivative of a part of the electronic wave function for two values of the separation constant A. (The correct value for A is 0.3486024)

condition that $\frac{dM}{d\mu}$ shall be finite restricts the value of A. However the analogue computations were too laborious and not accurate enough for our purpose. (2) was then solved by numerical integration, starting from $\mu = 0$. The calculated sign of $\frac{d^2M}{d\mu^2}$ near $\mu = 1$ indicated whether A was too large or too small.

This method turned out to be still inefficient compared with a method followed by Hylleraas[9]. The function $M(\mu)$ is written as

$$M(\mu) = \sum_{\ell=0}^{\infty} c_\ell P_\ell(\mu)$$

$P_\ell(\mu)$ being Legendre functions. When using the recurrence relation

$$(1 - \mu^2) P_n''(\mu) - 2\mu P_n'(\mu) + n(n+1) P_n(\mu) = 0 \qquad \ldots (4)$$

(2) gives a recurrence relation* for c_ℓ

$$\frac{(\ell-1)\ell}{(2\ell-3)(2\ell-1)} p^2 c_{\ell-2} + \left\{ -A - \ell(\ell+1) + \left[\frac{(\ell+1)^2}{(2\ell+3)(2\ell+1)} + \frac{\ell^2}{(2\ell+1)(2\ell-1)} \right] p^2 \right\} c_\ell$$

$$+ \frac{(\ell+2)(\ell+1)}{(2\ell+5)(2\ell+3)} p^2 c_{\ell+2} = 0.$$

For $p = 0$ we find by subtracting (4) from (2) that $-A = n(n+1)$.

For the $1s\sigma_g$ state $A = 0$. Although for our problem only the ground state is of immediate interest we have also calculated the $2p\sigma_u$ state for which $A = -2$ since this involved only a small change in the computer program.

The recurrence relation is considered as an infinite set of homogeneous linear equations, in which the determinant of the coefficient matrix must be zero. This determinant contains p and A and, by equating it to zero, A is defined as a function of p. For the ground state ℓ is even, for ℓ odd we find the solution for the $2p\sigma_u$ state. Since this determinant has an infinite number of terms it is difficult to be certain of the number of terms which must be taken into account in order to achieve the required accuracy. However only diagonal and neighbouring terms exist and in view of the simplicity and speed of calculating such a determinant by computer, we have considered a 50 x 50 determinant (notation D(50))**. Taking into account only D (10) does in fact lead to exactly the same values of A as a function of p in 9 decimal places.

---

*There appears to be a misprint in the original paper by Hylleraas. In equation (9c) a factor C has been omitted in the last term on the left hand side.

**The computer used was the IBM 7030 (Stretch). The program was written in the S2 language, which is a dialect of Fortran 2.

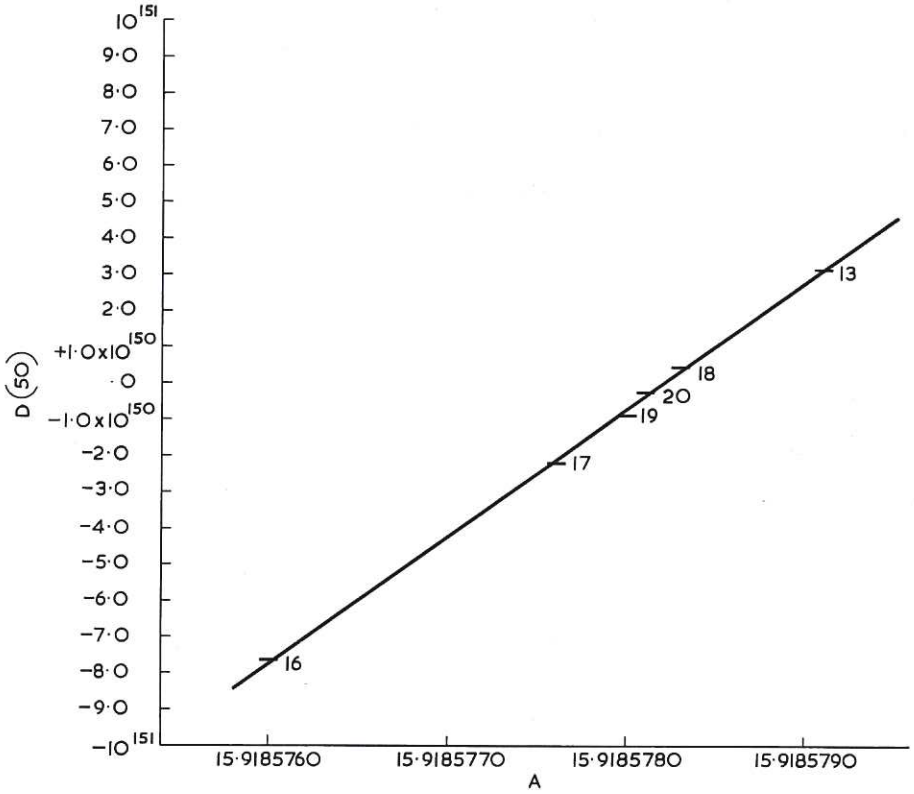

Fig. 4
D(50) as a function of A for P = 4.97979. The step numbers are also indicated

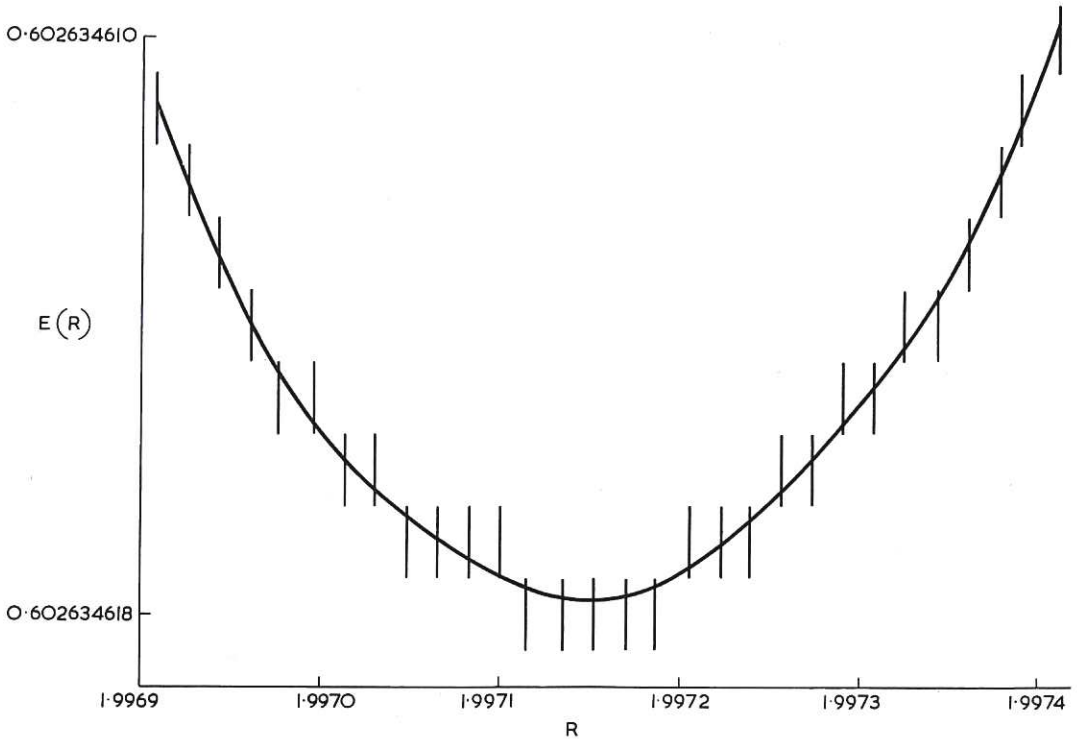

Fig. 5
The sum of electron energy and 1/R near the minimum

Fig.4 gives an example how D(50) varies as a function of A. It can be seen that D(50) is an extraordinarily steep function of A. In fact a change of 10^{-8} in A varies D(50) by 10^{150}.

Having calculated A as a function of p, we substitute these values in (3) and now calculate E as a function of p, or since $p^2 = -\frac{1}{2}R^2E$, E as a function of R. We follow the method given by Jaffe[10], putting

$$\Lambda(\lambda) = (\lambda + 1)^{\sigma} y[(\lambda - 1)/(\lambda + 1)]e^{-p\lambda},$$

in which $\sigma = \frac{R}{p} - 1$ and taking

$$y = \sum_{t=0}^{\infty} g_t \left(\frac{\lambda - 1}{\lambda + 1} \right)^t .$$

Then from (3) the following recurrence relation is found

$$(t - 1 - \sigma)^2 \, g_{t-1} - \left\{ 2t^2 + (4p - 2\sigma)\, t - A + p^2 - (2p + 1)\sigma \right\} g_t + (t + 1)^2 \, g_{t+1} = 0$$

We now consider this again as a coefficient matrix, the determinant of which must be zero. We have again taken D(50) into account although D(10) produces the same values of R. In either determinant, both that related to (2) and that related to (3), A and R respectively were adjusted until D(50) changed its sign when A and R changed by less than 10^{-9}.

For each state some 950 pairs of values for E and R were calculated. In order to calculate the minimum energy of the ground state when the $\frac{1}{R}$ term is added, successively smaller steps have been taken in the p values around the minimum found already. By doing this three times the following minimum value was found (see Fig.5).

$$E = -0.602634618 \pm 5 \times 10^{-10}$$

for

$$R = 1.99715 \pm 5 \times 10^{-6}$$

This is the energy calculated less accurately by, Burrau[8] and Hylleraas[9]. The value of R is so close to 2, that one would think that an approximation method would give 2 exactly. With the L C A O method however a minimum at R = 2.492830 is found (E = - 0.5648310).

Having calculated E for the R values determined by the value taken for p we then calculated E for values of R from 0.05 to 39.95 in steps of 0.05 by interpolation. To do so 8 neighbouring values of R for which E had been calculated were taken into account using 4 on each side. Through these 8 points a 7th power polynominal was fitted, and this was then used to calculate E for the specified values of R. To check the accuracy interpolations using 6, 10 and 12 points were also made for all the values of R. The difference between the values obtained using 6, 8, 10 or 12 points were in no case larger than 10^{-7}. The results for R up to 20 are presented in the tables I and II.

THE ENERGY E OF THE GROUND STATE OF AN ELECTRON IN THE FIELD OF TWO COULOMB-CENTRES WITH A SEPARATION R. (ATOMIC UNITS)

TABLE I

The $1S\sigma_g$ state

R	E	R	E	R	E	R	E
0.05	-1.9939765	5.05	-0.7216226	10.05	-0.6000615	15.05	-0.5664934
0.10	-1.9782421	5.10	-0.7188866	10.10	-0.5995499	15.10	-0.5662726
0.15	-1.9557214	5.15	-0.7162110	10.15	-0.5990439	15.15	-0.5660533
0.20	-1.9286202	5.20	-0.7135943	10.20	-0.5985434	15.20	-0.5658354
0.25	-1.8985570	5.25	-0.7110348	10.25	-0.5980483	15.25	-0.5656190
0.30	-1.8667039	5.30	-0.7085314	10.30	-0.5975584	15.30	-0.5654041
0.35	-1.8339027	5.35	-0.7060825	10.35	-0.5970738	15.35	-0.5651905
0.40	-1.8007539	5.40	-0.7036868	10.40	-0.5965943	15.40	-0.5649783
0.45	-1.7676828	5.45	-0.7013429	10.45	-0.5961198	15.45	-0.5647675
0.50	-1.7349879	5.50	-0.6990497	10.50	-0.5956503	15.50	-0.5645581
0.55	-1.7028754	5.55	-0.6968058	10.55	-0.5951855	15.55	-0.5643501
0.60	-1.6714846	5.60	-0.6946100	10.60	-0.5947256	15.60	-0.5641433
0.65	-1.6409064	5.65	-0.6924610	10.65	-0.5942703	15.65	-0.5639379
0.70	-1.6111962	5.70	-0.6903578	10.70	-0.5938197	15.70	-0.5637339
0.75	-1.5823827	5.75	-0.6882991	10.75	-0.5933735	15.75	-0.5635311
0.80	-1.5544801	5.80	-0.6862839	10.80	-0.5929319	15.80	-0.5633296
0.85	-1.5274832	5.85	-0.6843110	10.85	-0.5924946	15.85	-0.5631294
0.90	-1.5013815	5.90	-0.6823793	10.90	-0.5920616	15.90	-0.5629305
0.95	-1.4761568	5.95	-0.6804879	10.95	-0.5916329	15.95	-0.5627328
1.00	-1.4517863	6.00	-0.6786357	11.00	-0.5912083	16.00	-0.5625364
1.05	-1.4282441	6.05	-0.6768217	11.05	-0.5907879	16.05	-0.5623412
1.10	-1.4055027	6.10	-0.6750449	11.10	-0.5903715	16.10	-0.5621472
1.15	-1.3835336	6.15	-0.6733044	11.15	-0.5899590	16.15	-0.5619544
1.20	-1.3623078	6.20	-0.6715993	11.20	-0.5895505	16.20	-0.5617628
1.25	-1.3417965	6.25	-0.6699286	11.25	-0.5891459	16.25	-0.5615724
1.30	-1.3219714	6.30	-0.6682914	11.30	-0.5887450	16.30	-0.5613832
1.35	-1.3028046	6.35	-0.6666870	11.35	-0.5883479	16.35	-0.5611951
1.40	-1.2842692	6.40	-0.6651144	11.40	-0.5879545	16.40	-0.5610082
1.45	-1.2663393	6.45	-0.6635729	11.45	-0.5875647	16.45	-0.5608225
1.50	-1.2489899	6.50	-0.6620616	11.50	-0.5871784	16.50	-0.5606378
1.55	-1.2321968	6.55	-0.6605798	11.55	-0.5867957	16.55	-0.5604543
1.60	-1.2159372	6.60	-0.6591268	11.60	-0.5864165	16.60	-0.5602719
1.65	-1.2001891	6.65	-0.6577016	11.65	-0.5860407	16.65	-0.5600906
1.70	-1.1849316	6.70	-0.6563038	11.70	-0.5856682	16.70	-0.5599104
1.75	-1.1701446	6.75	-0.6549325	11.75	-0.5852991	16.75	-0.5597313
1.80	-1.1558092	6.80	-0.6535871	11.80	-0.5849332	16.80	-0.5595532
1.85	-1.1419072	6.85	-0.6522669	11.85	-0.5845706	16.85	-0.5593762
1.90	-1.1284216	6.90	-0.6509712	11.90	-0.5842112	16.90	-0.5592002
1.95	-1.1153358	6.95	-0.6496995	11.95	-0.5838549	16.95	-0.5590253
2.00	-1.1026342	7.00	-0.6484511	12.00	-0.5835016	17.00	-0.5588515
2.05	-1.0903021	7.05	-0.6472255	12.05	-0.5831515	17.05	-0.5586786
2.10	-1.0783254	7.10	-0.6460220	12.10	-0.5828043	17.10	-0.5585068
2.15	-1.0666907	7.15	-0.6448400	12.15	-0.5824601	17.15	-0.5583359
2.20	-1.0553851	7.20	-0.6436791	12.20	-0.5821189	17.20	-0.5581661
2.25	-1.0443965	7.25	-0.6425387	12.25	-0.5817805	17.25	-0.5579973
2.30	-1.0337135	7.30	-0.6414182	12.30	-0.5814449	17.30	-0.5578294
2.35	-1.0233249	7.35	-0.6403173	12.35	-0.5811122	17.35	-0.5576625
2.40	-1.0132203	7.40	-0.6392353	12.40	-0.5807823	17.40	-0.5574966
2.45	-1.0033897	7.45	-0.6381718	12.45	-0.5804551	17.45	-0.5573316
2.50	-0.9938235	7.50	-0.6371263	12.50	-0.5801306	17.50	-0.5571676
2.55	-0.9845127	7.55	-0.6360984	12.55	-0.5798087	17.55	-0.5570045
2.60	-0.9754486	7.60	-0.6350877	12.60	-0.5794895	17.60	-0.5568423
2.65	-0.9666229	7.65	-0.6340937	12.65	-0.5791729	17.65	-0.5566811
2.70	-0.9580277	7.70	-0.6331160	12.70	-0.5788588	17.70	-0.5565207
2.75	-0.9496554	7.75	-0.6321542	12.75	-0.5785473	17.75	-0.5563613
2.80	-0.9414989	7.80	-0.6312079	12.80	-0.5782383	17.80	-0.5562028
2.85	-0.9335511	7.85	-0.6302767	12.85	-0.5779317	17.85	-0.5560452
2.90	-0.9258056	7.90	-0.6293603	12.90	-0.5776276	17.90	-0.5558884
2.95	-0.9182560	7.95	-0.6284583	12.95	-0.5773259	17.95	-0.5557325
3.00	-0.9108962	8.00	-0.6275704	13.00	-0.5770266	18.00	-0.5555775
3.05	-0.9037204	8.05	-0.6266962	13.05	-0.5767296	18.05	-0.5554234
3.10	-0.8967231	8.10	-0.6258353	13.10	-0.5764349	18.10	-0.5552701
3.15	-0.8898988	8.15	-0.6249876	13.15	-0.5761425	18.15	-0.5551176
3.20	-0.8832426	8.20	-0.6241526	13.20	-0.5758524	18.20	-0.5549660
3.25	-0.8767494	8.25	-0.6233300	13.25	-0.5755646	18.25	-0.5548153
3.30	-0.8704145	8.30	-0.6225197	13.30	-0.5752789	18.30	-0.5546653
3.35	-0.8642334	8.35	-0.6217212	13.35	-0.5749954	18.35	-0.5545162
3.40	-0.8582017	8.40	-0.6209343	13.40	-0.5747141	18.40	-0.5543679
3.45	-0.8523152	8.45	-0.6201587	13.45	-0.5744349	18.45	-0.5542204
3.50	-0.8465698	8.50	-0.6193942	13.50	-0.5741578	18.50	-0.5540737
3.55	-0.8409617	8.55	-0.6186406	13.55	-0.5738828	18.55	-0.5539277
3.60	-0.8354871	8.60	-0.6178975	13.60	-0.5736098	18.60	-0.5537826
3.65	-0.8301423	8.65	-0.6171648	13.65	-0.5733389	18.65	-0.5536383
3.70	-0.8249238	8.70	-0.6164422	13.70	-0.5730700	18.70	-0.5534947
3.75	-0.8198284	8.75	-0.6157294	13.75	-0.5728031	18.75	-0.5533519
3.80	-0.8148526	8.80	-0.6150264	13.80	-0.5725381	18.80	-0.5532098
3.85	-0.8099934	8.85	-0.6143327	13.85	-0.5722751	18.85	-0.5530685
3.90	-0.8052476	8.90	-0.6136484	13.90	-0.5720140	18.90	-0.5529280
3.95	-0.8006124	8.95	-0.6129730	13.95	-0.5717548	18.95	-0.5527882
4.00	-0.7960849	9.00	-0.6123066	14.00	-0.5714975	19.00	-0.5526492
4.05	-0.7916623	9.05	-0.6116487	14.05	-0.5712421	19.05	-0.5525108
4.10	-0.7873419	9.10	-0.6109994	14.10	-0.5709884	19.10	-0.5523732
4.15	-0.7831211	9.15	-0.6103584	14.15	-0.5707366	19.15	-0.5522363
4.20	-0.7789974	9.20	-0.6097254	14.20	-0.5704866	19.20	-0.5521002
4.25	-0.7749684	9.25	-0.6091005	14.25	-0.5702384	19.25	-0.5519647
4.30	-0.7710317	9.30	-0.6084833	14.30	-0.5699919	19.30	-0.5518300
4.35	-0.7671849	9.35	-0.6078738	14.35	-0.5697472	19.35	-0.5516959
4.40	-0.7634259	9.40	-0.6072717	14.40	-0.5695042	19.40	-0.5515625
4.45	-0.7597524	9.45	-0.6066769	14.45	-0.5692628	19.45	-0.5514299
4.50	-0.7561623	9.50	-0.6060894	14.50	-0.5690232	19.50	-0.5512979
4.55	-0.7526535	9.55	-0.6055088	14.55	-0.5687852	19.55	-0.5511665
4.60	-0.7492241	9.60	-0.6049352	14.60	-0.5685489	19.60	-0.5510359
4.65	-0.7458721	9.65	-0.6043683	14.65	-0.5683142	19.65	-0.5509059
4.70	-0.7425955	9.70	-0.6038080	14.70	-0.5680812	19.70	-0.5507766
4.75	-0.7393926	9.75	-0.6032543	14.75	-0.5678497	19.75	-0.5506479
4.80	-0.7362615	9.80	-0.6027069	14.80	-0.5676198	19.80	-0.5505199
4.85	-0.7332004	9.85	-0.6021658	14.85	-0.5673914	19.85	-0.5503925
4.90	-0.7302076	9.90	-0.6016308	14.90	-0.5671646	19.90	-0.5502658
4.95	-0.7272814	9.95	-0.6011018	14.95	-0.5669394	19.95	-0.5501397
5.00	-0.7244203	10.00	-0.6005787	15.00	-0.5667156	20.00	-0.5500143

THE ENERGY E OF THE FIRST EXCITED STATE OF AN ELECTRON IN THE FIELD OF TWO COULOMB-CENTRES WITH A SEPARATION R. (ATOMIC UNITS)

TABLE II

The $2P\sigma_u$ state

R	E	R	E	R	E	R	E
0.05	-0.5001667	5.05	-0.6762862	10.05	-0.5994135	15.05	-0.5664868
0.10	-0.5006675	5.10	-0.6752785	10.10	-0.5969304	15.10	-0.5662643
0.15	-0.5015037	5.15	-0.6742691	10.15	-0.5944516	15.15	-0.5660473
0.20	-0.5026774	5.20	-0.6732586	10.20	-0.5919772	15.20	-0.5658297
0.25	-0.5041909	5.25	-0.6722475	10.25	-0.5895070	15.25	-0.5656136
0.30	-0.5060459	5.30	-0.6712364	10.30	-0.5870410	15.30	-0.5653989
0.35	-0.5082437	5.35	-0.6702258	10.35	-0.5845791	15.35	-0.5651855
0.40	-0.5107842	5.40	-0.6692161	10.40	-0.5821214	15.40	-0.5649736
0.45	-0.5136660	5.45	-0.6682078	10.45	-0.5796678	15.45	-0.5647630
0.50	-0.5168855	5.50	-0.6672013	10.50	-0.5772182	15.50	-0.5645538
0.55	-0.5204365	5.55	-0.6661970	10.55	-0.5747725	15.55	-0.5643459
0.60	-0.5243104	5.60	-0.6651953	10.60	-0.5723308	15.60	-0.5641394
0.65	-0.5284951	5.65	-0.6641964	10.65	-0.5698930	15.65	-0.5639342
0.70	-0.5329755	5.70	-0.6632008	10.70	-0.5674590	15.70	-0.5637303
0.75	-0.5377331	5.75	-0.6622087	10.75	-0.5650288	15.75	-0.5635277
0.80	-0.5427459	5.80	-0.6612204	10.80	-0.5626024	15.80	-0.5633264
0.85	-0.5479892	5.85	-0.6602362	10.85	-0.5601797	15.85	-0.5631263
0.90	-0.5534352	5.90	-0.6592564	10.90	-0.5577607	15.90	-0.5629275
0.95	-0.5590539	5.95	-0.6582811	10.95	-0.5553453	15.95	-0.5627300
1.00	-0.5648136	6.00	-0.6573106	11.00	-0.5529335	16.00	-0.5625337
1.05	-0.5706816	6.05	-0.6563450	11.05	-0.5505253	16.05	-0.5623386
1.10	-0.5766243	6.10	-0.6553847	11.10	-0.5481205	16.10	-0.5621447
1.15	-0.5826089	6.15	-0.6544297	11.15	-0.5457192	16.15	-0.5619521
1.20	-0.5886027	6.20	-0.6534802	11.20	-0.5433214	16.20	-0.5617606
1.25	-0.5945749	6.25	-0.6525363	11.25	-0.5409269	16.25	-0.5615703
1.30	-0.6004961	6.30	-0.6515983	11.30	-0.5385358	16.30	-0.5613812
1.35	-0.6063393	6.35	-0.6506662	11.35	-0.5361480	16.35	-0.5611932
1.40	-0.6120800	6.40	-0.6497401	11.40	-0.5337635	16.40	-0.5610064
1.45	-0.6176960	6.45	-0.6488201	11.45	-0.5313822	16.45	-0.5608207
1.50	-0.6231682	6.50	-0.6479065	11.50	-0.5290041	16.50	-0.5606361
1.55	-0.6284799	6.55	-0.6469991	11.55	-0.5266291	16.55	-0.5604527
1.60	-0.6336173	6.60	-0.6460982	11.60	-0.5242573	16.60	-0.5602704
1.65	-0.6385690	6.65	-0.6452037	11.65	-0.5218886	16.65	-0.5600891
1.70	-0.6433259	6.70	-0.6443159	11.70	-0.5195230	16.70	-0.5599090
1.75	-0.6478815	6.75	-0.6434346	11.75	-0.5171603	16.75	-0.5597299
1.80	-0.6522311	6.80	-0.6425600	11.80	-0.5148007	16.80	-0.5595519
1.85	-0.6563717	6.85	-0.6416920	11.85	-0.5124440	16.85	-0.5593750
1.90	-0.6603021	6.90	-0.6408309	11.90	-0.5100902	16.90	-0.5591991
1.95	-0.6640225	6.95	-0.6399765	11.95	-0.5077393	16.95	-0.5590242
2.00	-0.6675344	7.00	-0.6391288	12.00	-0.5053912	17.00	-0.5588504
2.05	-0.6708403	7.05	-0.6382881	12.05	-0.5030460	17.05	-0.5586776
2.10	-0.6739435	7.10	-0.6374541	12.10	-0.5007036	17.10	-0.5585058
2.15	-0.6768482	7.15	-0.6366270	12.15	-0.4983639	17.15	-0.5583350
2.20	-0.6795592	7.20	-0.6358067	12.20	-0.4960269	17.20	-0.5581652
2.25	-0.6820817	7.25	-0.6349933	12.25	-0.4936927	17.25	-0.5579964
2.30	-0.6844213	7.30	-0.6341868	12.30	-0.4913611	17.30	-0.5578286
2.35	-0.6865839	7.35	-0.6333871	12.35	-0.4890321	17.35	-0.5576617
2.40	-0.6885758	7.40	-0.6325942	12.40	-0.4867058	17.40	-0.5574958
2.45	-0.6904030	7.45	-0.6318082	12.45	-0.4843820	17.45	-0.5573309
2.50	-0.6920721	7.50	-0.6310290	12.50	-0.4820608	17.50	-0.5571669
2.55	-0.6935892	7.55	-0.6302565	12.55	-0.4797421	17.55	-0.5570048
2.60	-0.6949607	7.60	-0.6294909	12.60	-0.4774258	17.60	-0.5568417
2.65	-0.6961929	7.65	-0.6287320	12.65	-0.4751121	17.65	-0.5566805
2.70	-0.6972919	7.70	-0.6279798	12.70	-0.4728008	17.70	-0.5565202
2.75	-0.6982638	7.75	-0.6272343	12.75	-0.4704919	17.75	-0.5563608
2.80	-0.6991145	7.80	-0.6264954	12.80	-0.4681853	17.80	-0.5562023
2.85	-0.6998498	7.85	-0.6257632	12.85	-0.4658812	17.85	-0.5560447
2.90	-0.7004753	7.90	-0.6250376	12.90	-0.4635793	17.90	-0.5558879
2.95	-0.7009964	7.95	-0.6243185	12.95	-0.4612798	17.95	-0.5557321
3.00	-0.7014163	8.00	-0.6236060	13.00	-0.4589825	18.00	-0.5555771
3.05	-0.7017462	8.05	-0.6229000	13.05	-0.4566875	18.05	-0.5554230
3.10	-0.7019849	8.10	-0.6222003	13.10	-0.4543948	18.10	-0.5552697
3.15	-0.7021391	8.15	-0.6215071	13.15	-0.4521042	18.15	-0.5551173
3.20	-0.7022134	8.20	-0.6208202	13.20	-0.4498158	18.20	-0.5549657
3.25	-0.7022120	8.25	-0.6201397	13.25	-0.4475296	18.25	-0.5548149
3.30	-0.7021392	8.30	-0.6194654	13.30	-0.4452455	18.30	-0.5546650
3.35	-0.7019908	8.35	-0.6187973	13.35	-0.4429635	18.35	-0.5545159
3.40	-0.7017948	8.40	-0.6181353	13.40	-0.4406836	18.40	-0.5543676
3.45	-0.7015367	8.45	-0.6174795	13.45	-0.4384058	18.45	-0.5542201
3.50	-0.7012100	8.50	-0.6168298	13.50	-0.4361301	18.50	-0.5540734
3.55	-0.7008361	8.55	-0.6161861	13.55	-0.4338563	18.55	-0.5539275
3.60	-0.7004121	8.60	-0.6155483	13.60	-0.4315845	18.60	-0.5537824
3.65	-0.6999410	8.65	-0.6149165	13.65	-0.4293148	18.65	-0.5536381
3.70	-0.6994257	8.70	-0.6142905	13.70	-0.4270470	18.70	-0.5534945
3.75	-0.6988689	8.75	-0.6136704	13.75	-0.4247811	18.75	-0.5533517
3.80	-0.6982734	8.80	-0.6130560	13.80	-0.4225171	18.80	-0.5532097
3.85	-0.6976414	8.85	-0.6124473	13.85	-0.4202551	18.85	-0.5530684
3.90	-0.6969755	8.90	-0.6118442	13.90	-0.4179949	18.90	-0.5529278
3.95	-0.6962779	8.95	-0.6112468	13.95	-0.4157366	18.95	-0.5527880
4.00	-0.6955506	9.00	-0.6106549	14.00	-0.4134801	19.00	-0.5526490
4.05	-0.6947958	9.05	-0.6100686	14.05	-0.4112254	19.05	-0.5525107
4.10	-0.6940154	9.10	-0.6094876	14.10	-0.4089725	19.10	-0.5523731
4.15	-0.6932111	9.15	-0.6089121	14.15	-0.4067215	19.15	-0.5522362
4.20	-0.6923848	9.20	-0.6083419	14.20	-0.4044721	19.20	-0.5521000
4.25	-0.6915382	9.25	-0.6077769	14.25	-0.4022246	19.25	-0.5519646
4.30	-0.6906727	9.30	-0.6072172	14.30	-0.3999787	19.30	-0.5518298
4.35	-0.6897898	9.35	-0.6066627	14.35	-0.3977346	19.35	-0.5516958
4.40	-0.6888911	9.40	-0.6061133	14.40	-0.3954921	19.40	-0.5515624
4.45	-0.6879778	9.45	-0.6055690	14.45	-0.3932514	19.45	-0.5514297
4.50	-0.6870512	9.50	-0.6050297	14.50	-0.3910123	19.50	-0.5512978
4.55	-0.6861125	9.55	-0.6044953	14.55	-0.3887748	19.55	-0.5511664
4.60	-0.6851629	9.60	-0.6039659	14.60	-0.3865389	19.60	-0.5510356
4.65	-0.6842035	9.65	-0.6034413	14.65	-0.3843047	19.65	-0.5509058
4.70	-0.6832352	9.70	-0.6029215	14.70	-0.3820720	19.70	-0.5507765
4.75	-0.6822591	9.75	-0.6024065	14.75	-0.3798410	19.75	-0.5506478
4.80	-0.6812761	9.80	-0.6018962	14.80	-0.3776115	19.80	-0.5505198
4.85	-0.6802870	9.85	-0.6013906	14.85	-0.3753835	19.85	-0.5503925
4.90	-0.6792927	9.90	-0.6008896	14.90	-0.3731571	19.90	-0.5502657
4.95	-0.6782940	9.95	-0.6003931	14.95	-0.3709321	19.95	-0.5501397
5.00	-0.6772916	10.00	-0.5999011	15.00	-0.3687087	20.00	-0.5500142

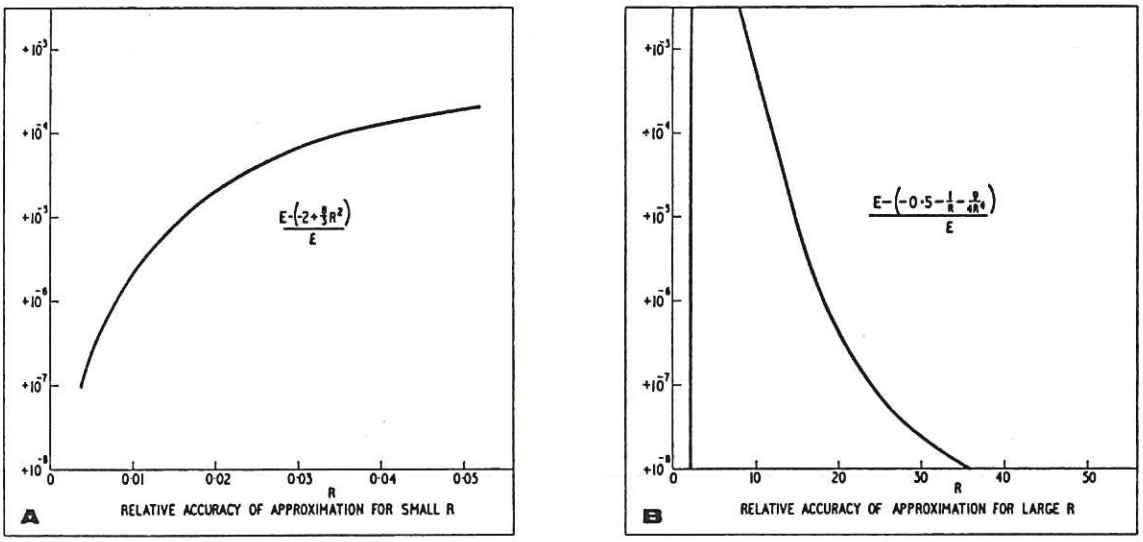

Fig. 6
The results of the calculation are compared with results obtained from two approximations, (a) for small and (b) for large values of R. It can be seen that in both cases the approximations become exact

For interpolation between even more points, always fitting an (n - 1)th power polynominal through n points, we found the accuracy decreasing. There appears in general to be an optimum number of points for the highest accuracy if the points have a finite accuracy and are not equi-distant. If the points are equi-distant the accuracy can in general be expected to increase with the number of points. We cannot prove this last statement but doing the test of calculating the original E values from the equi-distant ones, we found this to be the case.

For small values of R the system can be considered as a perturbed He^+ ion. Bethe[23] has calculated that in this case the energy of the ground state varies like $-2 + \frac{8}{3} R^2$. We have also calculated the energy for some 500 values of $R < 0.05$. Fig.6a shows the accuracy of this approximation.

For larger R the H_2^+ ion consists essentially of a hydrogen atom in the ground state (energy - 0.5) and a separated proton. Since the field at the atom produced by the proton is $F = \frac{1}{R^2}$, the energy due to the Stark shift of the ground state of the atom is $-\frac{9}{4R^4}$. The energy of the two protons is $+\frac{1}{R}$, so that the electron energy for large R will aproach

$$-0.5 - \frac{1}{R} - \frac{9}{4R^4} \quad .$$

Fig.6b shows the accuracy of this approximation.

In the table given by Cohen et al.[12], the energy varies more like $-0.5 - \frac{1}{R} - \frac{2}{R^4}$ for large R. This may be due to the method of approximation used in their calculations.

The difference between the two states calculated approaches $2(1 + R)e^{-R}$ for large R. This is also obtained from the L C A O approximation, even though this approximation does not give the $\frac{9}{4R^4}$ term since this term drops out in the difference between the two energies.

2.4 The Energy Levels

In section 2.2 we used the Born-Oppenheimer approximation: that is, we neglected the effect of the nuclear motion on the electron energy. This seemed justified since the reduced nuclear mass is roughly a thousand times heavier than the electron mass. However, as we have seen (1.3), the final accuracy of the calculation must be 10^{-5} for the error in the binding energy to be not more than a few per cent. The motion of the nuclei must therefore be taken into account as a first order perturbation. In general the first order perturbation hamiltonian H' is $\int \varphi\ (r)\ H'\ \varphi^*\ (r)\ dr$. We therefore expect the perturbation energy to be $g_{oo}(R_n) = \int \psi\ (R_e, R_n)\ \nabla_n^2\ \psi\ (R_e, R_n)\ dR_e$. This is indeed the correct value even though this is not immediately obvious since in our case the hamiltonian consists of two parts. A correct calculation[24] gives the same result. We have used the values of $g_{oo}(R_n)$ calculated by Cohen et. al[12]. The estimated error is 10^{-5}, which results in an error of less than 10^{-8} in the potential. By inclusion of the term the equation from 2.2 now takes the following form

$$\nabla^2\ \Pi(R) + \left\{ \frac{2M_n}{M_e}\left[W - E(R_n) - \frac{1}{R}\right] - \frac{J(J+1)}{R^2} - g_{oo}\ (R) \right\} \Pi(R) = 0$$

To simplify we write $y''(x) + f\ (x)y(x) = 0$. To solve this equation numerically for the eigen energies it is necessary first to specify the initial conditions. The true values $y(0) = y'(0) = 0$ would obviously give $y\ (x) = 0$. Moreover, starting from $x = 0$, we have to divide by 0. We therefore chose the initial conditions $x = 10^{-30}$; $y(x) = 0$; $y'(x) = 10^{-60}$. Since the normalisation is of no importance for the calculation of the eigen energy, the initial value of $y'(x)$ is irrelevant provided it is not zero, and it is not sufficiently large for the resulting $y(x)$ to have a maximum larger than 10^{309}, the largest number the computer can cope with. Changing the initial x to 10^{-60} leads to a change in the eigen energy of 10^{-8}. For the integration we first used the Runge-Kutta method[25].

This method has the advantage of giving an estimate of the error for each step, so that the step length can be adjusted accordingly. Its disadvantage is that the functions $E(R_n)$

and $g_{oo}(R_n)$ must be known for random values of R_n, as evaluated during the calculations. Interpolation was therefore used between eight known values, a procedure which took by far the greatest proportion of the computer time spent on this problem.

When the length of the steps was reduced from 0.025 to 0.01, the eigen-energy was found to change by 10^{-8}. This gives an indication of the accuracy. The method was used for the v = 18, J = 3 level only. A much faster method consisted in calculating 4000 values of E, (i.e. for steps of 0.01 in R), which were then stored on tape and used for each calculation. The integration was effected by fitting a parabola, satisfying $y_2'' = - f_2 y_2$, through the two proceding points (x_1, y_1) and (x_2, y_2). We thus took $y_3 = [2 - (dx)^2 f_2]y_2 - y_1$. Although this method was faster by an order of magnitude, the accuracy was found to be insufficient. Rather than reduce the step length a more accurate method of integration was used.

In addition to the information used in the above method, we know also that $y_1'' = - f_1 y_1$ and $y_3'' = - f_3 y_3$. We can therefore apply a 4th power polynominal which satisfies the equations:

$$
\begin{aligned}
y_1 &= ax_1^4 + bx_1^3 + cx_1^2 + dx_1 + e \\
y_2 &= ax_2^4 + bx_2^3 + cx_2^2 + dx_2 + e \\
y_3 &= ax_3^4 + bx_2^3 + cx_3^2 + dx_3 + e \\
-f_1 y_1 &= 12ax_1^2 + 6bx_1 + 2c \\
-f_2 y_2 &= 12ax_2^2 + 6bx_2 + 2c \\
-f_3 y_3 &= 12ax_3^2 + 6bx_3 + 2c
\end{aligned}
$$

where y_3 is unknown. We consider this set as 6 equations with 5 unknowns, that is a, b, c, d and e. In order to be solveable the determinant of the coefficient matrix must be zero, which enables us to find y_3 without knowing a, b, c, d and e. If we assume that $x_1 = x - h$; $x_2 = x$; $x_3 = x + h$ this determinant is

$$
\begin{vmatrix}
y_1 & (x-h)^4 & (x-h)^3 & (x-h)^2 & (x-h) & 1 \\
y_2 & x^4 & x^3 & x^2 & x & 1 \\
y_3 & (x+h)^4 & (x+h)^3 & (x+h)^2 & (x+h) & 1 \\
-f_1 y_1 & 12(x-h)^2 & 6(x-h) & 2 & 0 & 0 \\
-f_2 y_2 & 12x^2 & 6x & 2 & 0 & 0 \\
-f_3 y_3 & 12(x+h)^2 & 6(x+h) & 2 & 0 & 0
\end{vmatrix} = 0
$$

This can be reduced to:

$$\begin{vmatrix} y_1 & h^2 & -h^2 & h^2 & -h & 1 \\ y_2 & 0 & 0 & 0 & 0 & 1 \\ y_3 & h^2 & h^2 & h^2 & h & 1 \\ -f_1y_1 & 12 & -6 & 2 & 0 & 0 \\ -f_2y_2 & 0 & 0 & 2 & 0 & 0 \\ -f_3y_3 & 12 & 6 & 2 & 0 & 0 \end{vmatrix}$$

which leads to

$$y_3 = \frac{(24 - 10h^2f_2)y_2 - (12 + h^2f_1)y_1}{12 + h^2f_3}$$

In each method the integration was continued until, by the criteria given in Fig.7, it was possible to decide on the adjustment of the energy necessary for it to approach the eigen energy. After a series of decreasing adjustments finally the change in energy was less than 10^{-8}. This was done for values of the rotational quantum number up to J = 8. The results are presented in Table III. During the calculations the unit of energy was

$$\frac{1}{1 + m/2M} \cdot \frac{e^4}{(4\pi\varepsilon)^2\hbar^2}$$

so that the results had to be multiplied by 0.499864 to obtain atomic units. In Hiskes' table the "atomic Rydberg" is used: this is

$$\frac{1}{2} \cdot \frac{m}{1 + m/M} \cdot \frac{e^4}{(4\pi\varepsilon)^2\hbar^2} = 0.499728 \ .$$

His values agree with ours to 2×10^{-4} a.u. which is indeed the accuracy he claims. We believe our results to have an accuracy of 10^{-7} a.u. for the binding energies of the top levels.

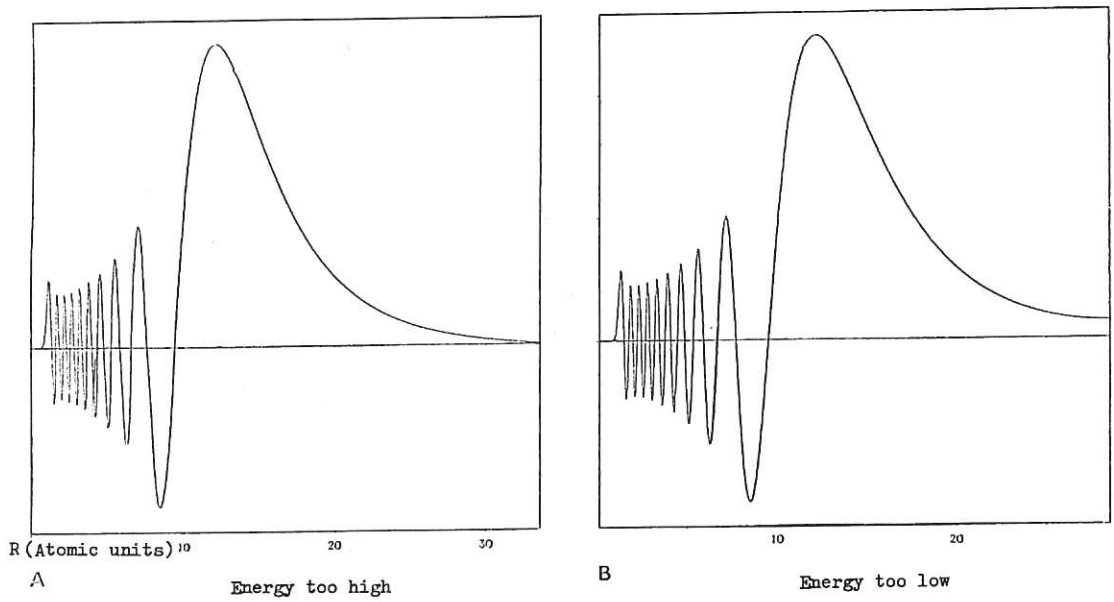

Fig. 7
The nuclear part of the wave function for the v = 18, J = 3 level just above and below the correct eigen energy

TABLE III

Energy levels of H_2^+ for various vibrational quantum number v, and rotational quantum number J. Atomic units are used

J	0	1	2	3	4
v					
0	-0.59713932	-0.59687398	-0.59634540	-0.59555777	-0.59451722
1	-0.58715483	-0.58690345	-0.58640272	-0.58565665	-0.58467109
2	-0.57775005	-0.57751216	-0.57703833	-0.57633239	-0.57539998
3	-0.56890573	-0.56868092	-0.56823318	-0.56756618	-0.56668531
4	-0.56060565	-0.56039359	-0.55997125	-0.55934218	-0.55851158
5	-0.55283645	-0.55263686	-0.55223940	-0.55164748	-0.55086609
6	-0.54558772	-0.54540041	-0.54502743	-0.54447208	-0.54373914
7	-0.53885193	-0.53867676	-0.53832801	-0.53780886	-0.53712394
8	-0.53262447	-0.53246140	-0.53213679	-0.53165372	-0.53101666
9	-0.52690388	-0.52675294	-0.52645255	-0.52600568	-0.52541668
10	-0.52169191	-0.52155322	-0.52127731	-0.52086705	-0.52032670
11	-0.51699381	-0.51686762	-0.51661667	-0.51624377	-0.51575309
12	-0.51281871	-0.51270538	-0.51248012	-0.51214572	-0.51170627
13	-0.50918001	-0.50908006	-0.50888154	-0.50858725	-0.50820124
14	-0.50609594	-0.50601008	-0.50583977	-0.50558781	-0.50525835
15	-0.50359010	-0.50351932	-0.50337921	-0.50317268	-0.50290406
16	-0.50169188	-0.50163753	-0.50153040	-0.50137362	-0.50117191
17	-0.50043456	-0.50039855	-0.50032833	-0.50022754	-0.50010186
18	-0.49983658	-0.49982099	-0.49979211	-0.49975483	-
19	-0.49973177	-0.49972943	-	-	-

J	5	6	7	8
v				
0	-0.59323169	-0.59171070	-0.58996523	-0.58800737
1	-0.58345367	-0.58201350	-0.58036108	-0.57850800
2	-0.57424837	-0.57288634	-0.57132391	-0.56957220
3	-0.56559759	-0.56431141	-0.56283640	-0.56118322
4	-0.55748613	-0.55627393	-0.55488424	-0.55332727
5	-0.54990168	-0.54876202	-0.54745601	-0.54599351
6	-0.54283486	-0.54176671	-0.54054327	-0.53917404
7	-0.53627925	-0.53528202	-0.53414054	-0.53286400
8	-0.53023143	-0.52930502	-0.52824546	-0.52706168
9	-0.52469119	-0.52383601	-0.52285896	-0.52176873
10	-0.51966174	-0.51887882	-0.51798557	-0.51699054
11	-0.51515001	-0.51444106	-0.51363377	-0.51273659
12	-0.51116710	-0.51053470	-0.50981657	-0.50902116
13	-0.50772890	-0.50717670	-0.50655228	-0.50586425
14	-0.50485686	-0.50439001	-0.50386570	-0.50329301
15	-0.50257907	-0.50220484	-0.50178993	-0.50134441
16	-0.50093162	-0.50066088	-0.50036983	-0.50007128
17	-0.49995928	-0.49981112	-	-

2.5 Dissociation Probability as a Function of Field

Having calculated the energy levels we now want to know the field required for dissociation. We first make a simple classical calculation. We note that the field has two effects: it not only enhances dissociation but the H_2^+ particle as a whole is accelerated. This results in only half the field acting on the potential between the two nuclei. This can easily be shown if we assume that the H_2^+ consists of a charged part with mass M and a neutral part with the same mass. The acceleration due to a field F is $a = eF/2M$. The force eF_{eff} acting between the two parts is therefore $eF_{eff} = Ma = eF/2$.

In the region of interest the energy difference with the dissociation limit is $9/4R^4$ (in the J = 0 case). When adding the effective field F_{eff} the potential becomes $V = -9/4R^4 - F_{eff}R$. Classically dissociation will occur if $E > V$. This gives $|E| < | 1.25 \times 9^{1/5} \times F_{eff}^{4/5}|$. If $J \geqslant 3$ the term $\frac{J(J+1)}{R^2} \frac{M_e}{2M_n}$ becomes comparable with $9/4R^4$ in the region of interest.

This classical picture leads however to an over estimation of the field because of the tunnelling effect; this means that even if the field is not high enough to make an energy level unbound the proton can still escape. To calculate this effect we use the transition probability derived from the W.K.B. approximation $\exp\left(-2\int_{r_2}^{r_3}\sqrt{2M_n\,(V-E)}\;dR\right)$ the integrant is real between r_2 and r_3, and

$$V = E_e\,(R) + 1/R + M_e\,J(J+1)/(2M_nR^2) + \tfrac{1}{2}\,F\,R$$

The probability current towards the barrier is

$$\left\{2\int_{r_1}^{r_2}\left[M_n\,(E-V)^{-\frac{1}{2}}\right]dR\right\}^{-1}$$

The integrant is real between r_1 and r_2.

The dissociation probability is therefore, in inverse atomic time units

$$P = \frac{\exp\left\{-2\int_{r_2}^{r_3}\left[2M_n\,(V-E)\right]^{\frac{1}{2}}dR\right\}}{2\int_{r_1}^{r_2}\left[M_n(E-V)^{-\frac{1}{2}}\right]dR}$$

Since the field acts only in one direction, we must now take the probability distribution of the orientation into account from 2.2, which is $2\pi \sin\theta\, Y^2_{J,m}(\theta)$.

The total dissociation probability (in inverse atomic time units) is now

$$P_t = \int_0^{\pi} 2\pi\, Y^2_{J,m}(\theta)\,\sin\theta\, P(F\cos\theta)\,d\theta$$

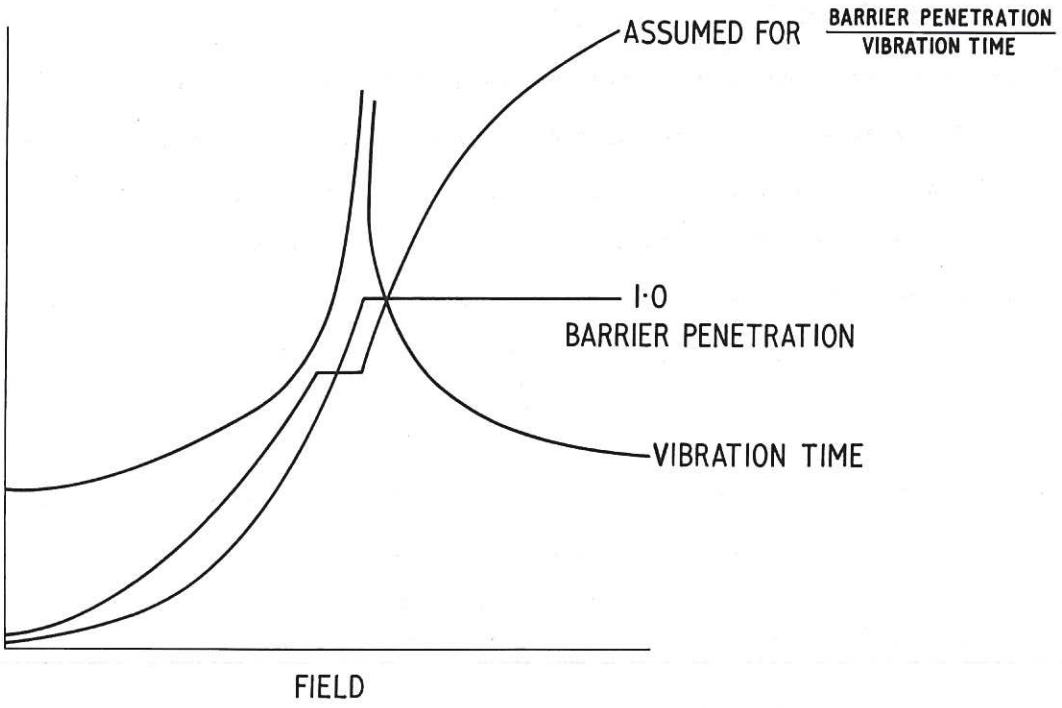

Fig. 8
Near the field for which the barrier is removed, the dissociation probability is assumed to be of the form indicated

To compute this integral steps of $\Delta R = 0.05$ were taken and for each level 200 values of P were evaluated for fields up to 10^5 V/cm in steps of 0.05×10^4 V/cm. Intermediate values were obtained by linear interpolation. The integration step in θ was $\pi/100$.

At the classical field necessary for dissociation, where $E = V(r_2)$, the denominator in the expression for P, the classical vibration time, becomes infinity and hence P would be zero. Since this is not physically acceptable, we have added the condition that P can only increase with F (see Fig.8). For values of F above the classical dissociation field, we have extended the integral in the denominator to the value of R for which V has a maximum. We then arrive at the dissociation probabilities given in Fig.9.

Fig. 10a gives the binding energies of the levels that are likely to be dissociated in fields below 10^5 V/cm. To compare the results with Hiskes' we derive the dissociation probability in $t = 10^{-8}$ sec $= 0.42 \times 10^9$ a.u. This is given by $1 - \exp(- P_t\, t)$. The results of the levels given by Hiskes[26] are given in Fig. 10b. The uncertainty he gave is a factor 2 for the threshold field and a factor 10 for the 18,0,0 level[27]. Our results for the same states are also given in Fig. 10 by the dashed curves. The error in our case is less than 10%. The improvement was made possible by calculating the electron energy to a higher accuracy.

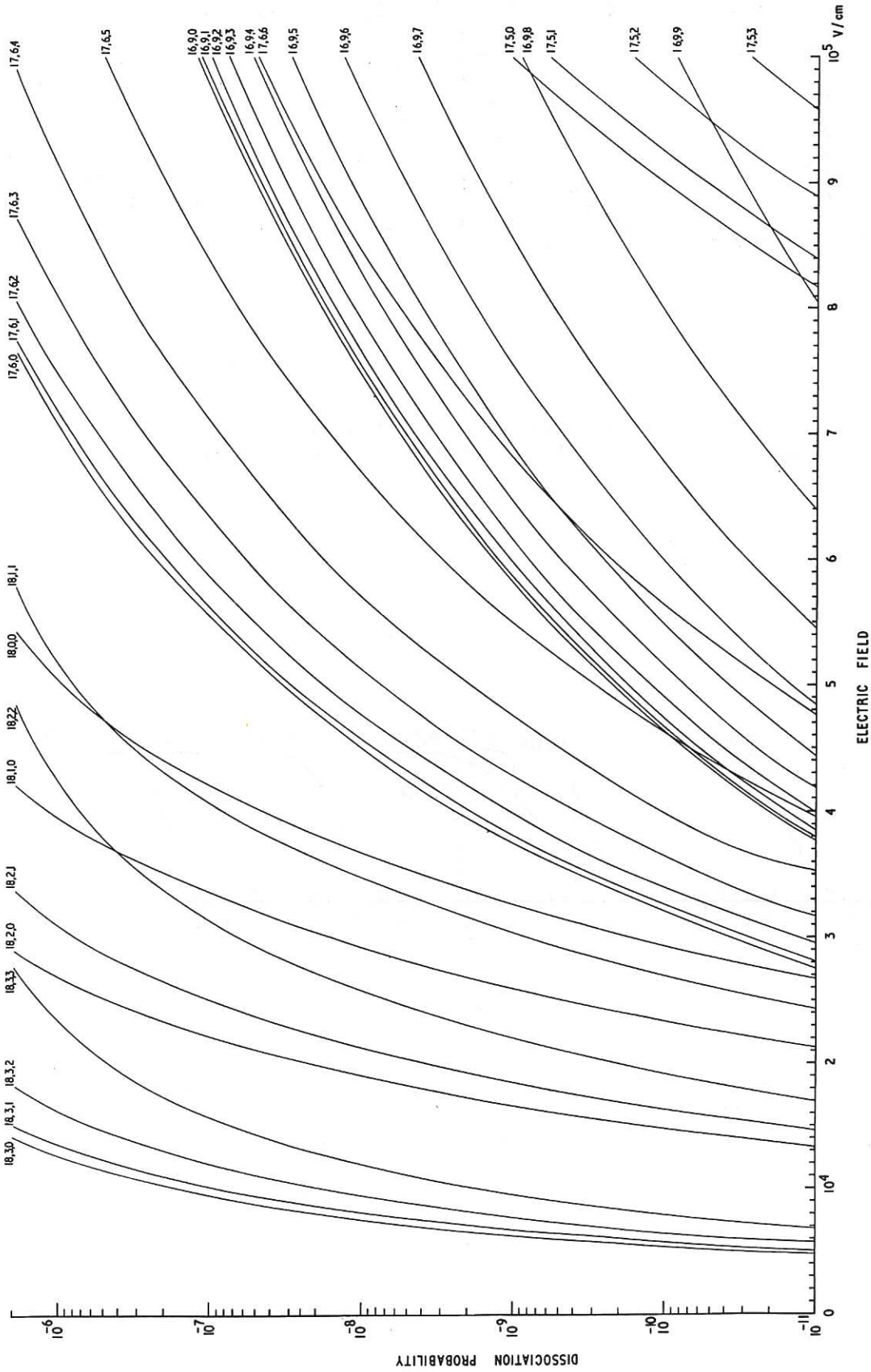

Fig. 9
The dissociation probability for the top levels in atomic units of time (2.4×10^{-17} sec)

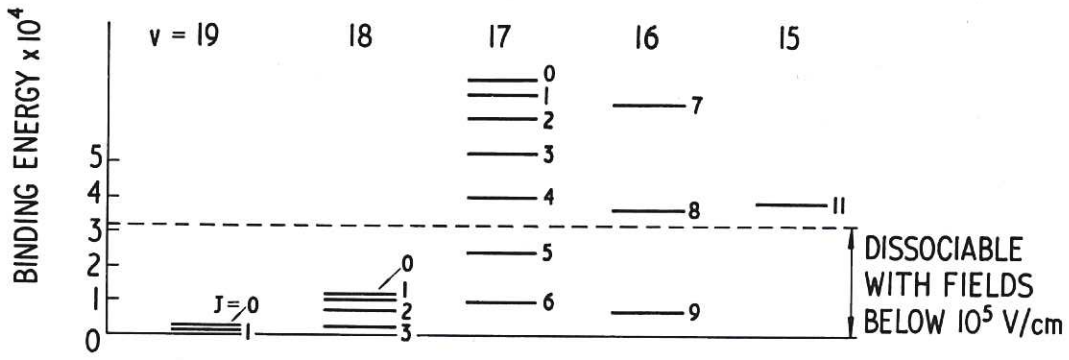

Fig. 10(a)
The levels which can theoretically be dissociated by fields below 10^5 v/cm. The binding energies of v = 19, being of order 10^{-6} a.u., are not drawn to scale

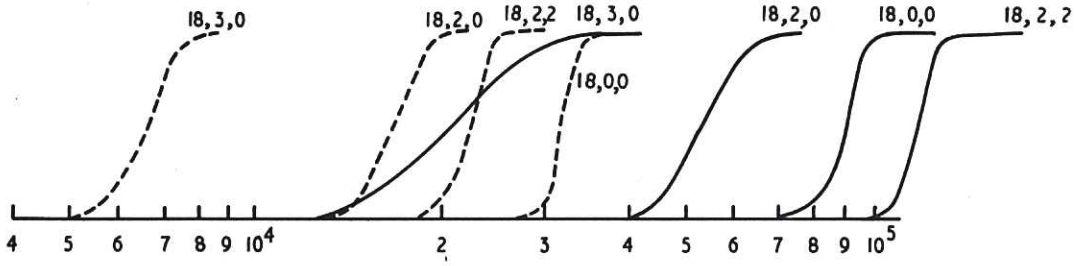

Fig. 10(b)
The probability of dissociation of the uppermost levels plotted as a function of electric field as given by Hiskes compared with the present work. These dissociation probabilities refer to an ion spending 10^{-8} sec in the field

PART II

In this part we will discuss the observations of field dissociation of H_2^+. We have used two experimental devices to do so, which are discussed in Chapters 3 and 4 respectively.

3. MEASUREMENT OF DISSOCIATION THRESHOLD AND DISSOCIATED FRACTION

3.1 H_2^+ Production

In the experiments to measure the dissociation of H_2^+ as a function of an applied electric field, a beam of H_2^+ ions was obtained from the break-up of H_3^+ ions (see 1.4). These ions were extracted from a radio-frequency ion source and accelerated to the required energy. After selecting the H_3^+ beam by bending it through 90^0, it is passed through a gas target in which the H_2^+ is formed. A second magnet then selects the H_2^+ by bending it through 10^0 (see Fig.11).

3.2 Choice of Energy

There is an advantage in using high particle energies because the dissociation cross-section on the residual gas is lower by about a factor 2 for 400 keV H_2^+ ions than for 100 keV H_2^+ ions.

A further advantage is that the detection of individual particles becomes easier at higher energies (see 3.5). Moreover, for the second device (see 4.4) the maximum attainable electric field is determined by the particle energy. On the other hand in both devices too high an energy would limit the minimum attainable field, because the particles are subjected to an equivalent electric field $\vec{F} = \vec{v} \times \vec{B}$ in the analysing magnets. Since the radius of curvature $r = mv/eB$ and the energy $eE = \frac{1}{2}mv^2$, the field $F = 2E/r$ and is thus proportional to the energy E.

Our experiments were performed mainly in the range of field strengths from $10^4 - 10^5$ V/cm. If H_2^+ were extracted direct from the source, the field in the 90^0 magnet would be equivalent to 10^4 V/cm for $E = \frac{10^4 \times 30}{2} = 150$ keV; the radius of curvature being 30 cm. But for H_2^+ from H_3^+ the 10^0 magnet, which selects H_2^+ after the gas target with a radius of curvature $r = 100$ cm, would limit the H_2^+ energy to $E = \frac{10^4 \times 100}{2} = 500$ keV corresponding to 750 keV H_3^+, which is unobtainable. The maximum energy available was 600 keV. However, in the first device the fringing field of a third magnet which selects H^0, H_2^+ and H^+ might cause dissociation of H_2^+ which would still result in detectable H^0 and H^+ counts. We have therefore taken various energies to eliminate this effect.

The magnetic fields were checked with a rotating coil with an accuracy of 2%.

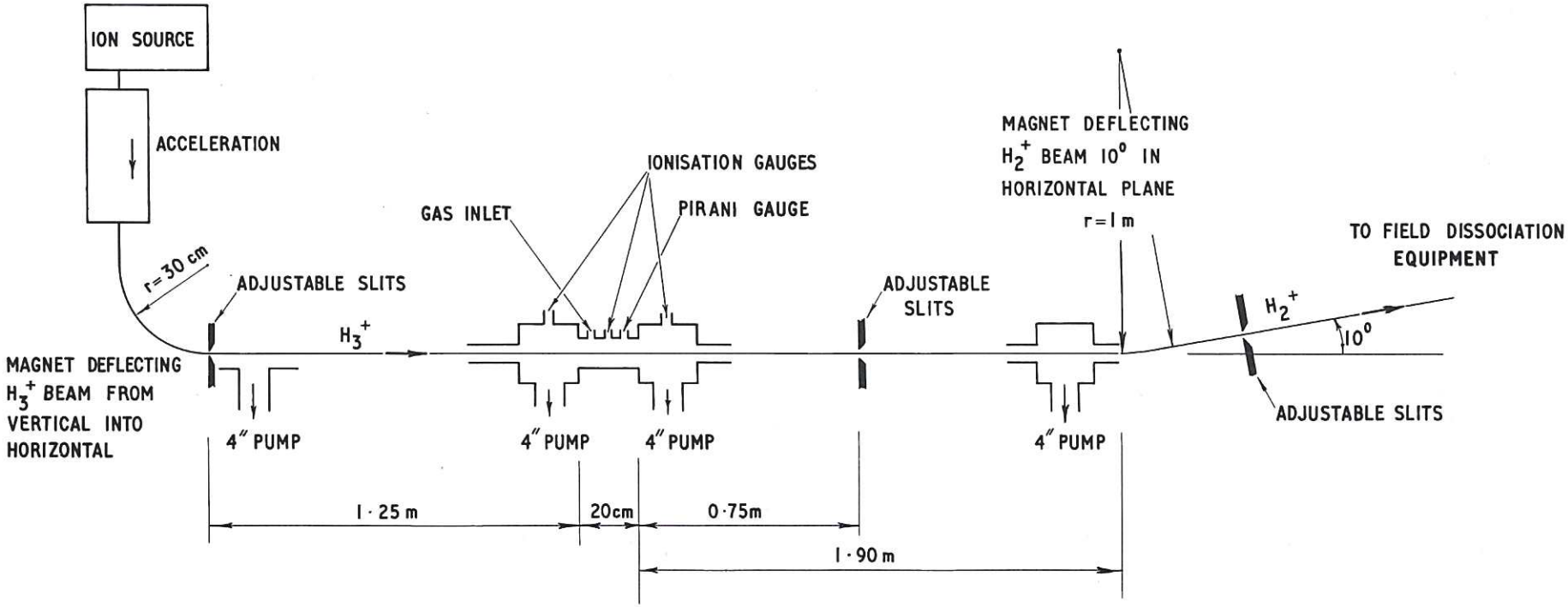

Fig. 11
The production of H_2^+ by the break up of H_3^+

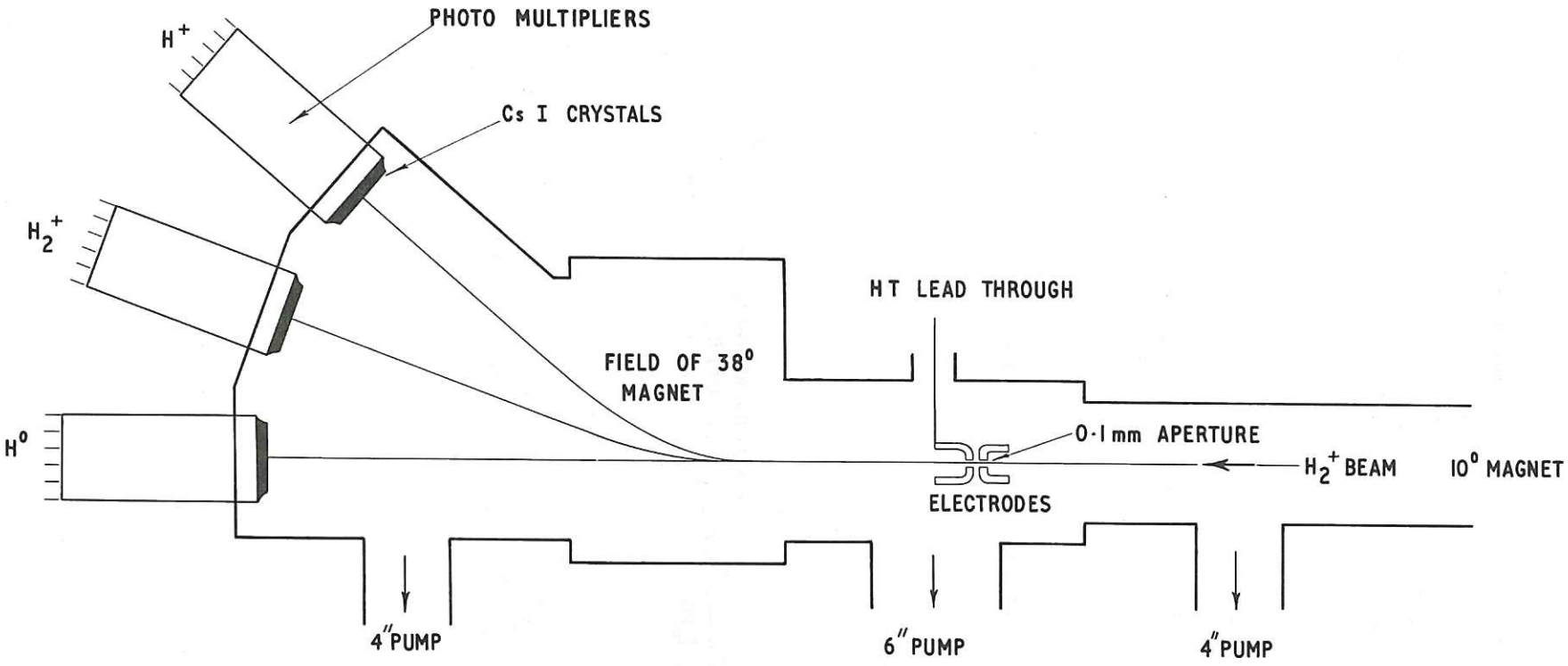

Fig. 12
The first device. An electric field is applied parallel to the beam and the dissociation products then analysed

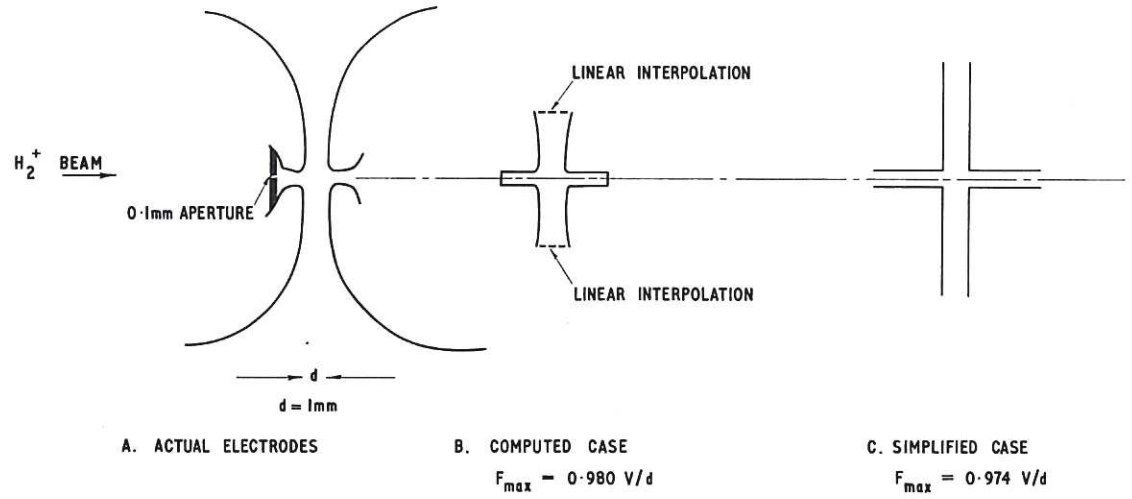

Fig. 13
The field produced by the actual electrodes (A) was computed for the shape given in B. For the simplified case C, the maximum field on the axis is given in Fig. 14

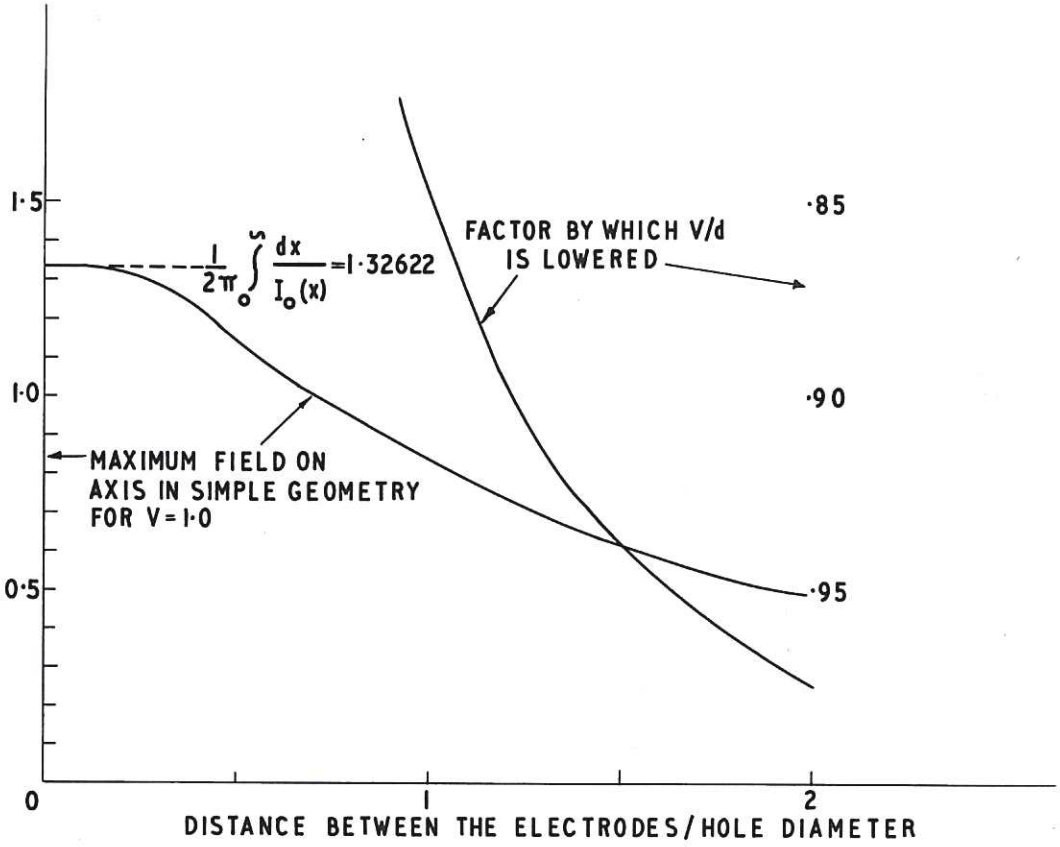

Fig. 14
The maximum field on the axis for the geometry given in Fig. 13 C

3.3 Description of the First Device

(Part of this has been published[28].)

A general picture of the first device is given in Fig. 12.

After selection of H_2^+ by the 10^o magnet the beam was passed through an electrode system similar to one used earlier by Riviere and Sweetman[14] in which an electric field is applied parallel to the direction of the ion beam over a variable distance of about 1 mm (see 3.4). The beam was then analysed into H^o, H_2^+ and H^+ by the 38^o magnet (H^+ is deflected through 38^o) and the particles were individually detected on CsI scintillation counters (3.5).

3.4 The Electrodes

Fig. 13a gives the dimensions of the electrodes used. The maximum field on the axis is obviously not simply V/d since it is weakened by the two holes and the rounded corners to, say, α V/d. To compute the actual field a relaxation method was used at some 5000 points. To do so, the electrodes were approximated by some 300 points on a 0.0254 mm mesh (see Fig. 13b). At 2.54 mm from the axis a linear potential was assumed. This gave a value of α, the correction factor of 0.980.

To extend this problem to a more general case, the maximum field on the axis in a geometry represented by Fig. 13c was computed as a function of the gap d in units of the potential difference and the hole diameter. The results are given in Fig. 14. The value for d = 0 can be calculated analytically[29] as $1/(2\pi) \int_0^\infty dx/I_o(x)$. We computed this to 1.32622.

When applying these results to the actual electrodes (d = 1 mm, hole diameter = 0.52mm) we find α = 0.974.

The gap was measured with a microscope with an accuracy of 0.025 mm or 2.5% so that it is immaterial whether α is 0.980 or 0.974.

The voltage was measured with a digital voltmeter and a potential divider with accuracies of 10^{-4} and 5×10^{-3} respectively.

3.5 The Scintillation Detector

The detectors used were EMI 2" photomultipliers on which a CsI crystal was attached with paraffin wax. Fig. 15 gives the circuit used which is the same as used by Riviere[30]. It can be used for detecting individual particles. Pulse height analysis showed that for 40 keV, H^+ and H^o are well resolved (see Fig. 16). When the beam is too intense for counting

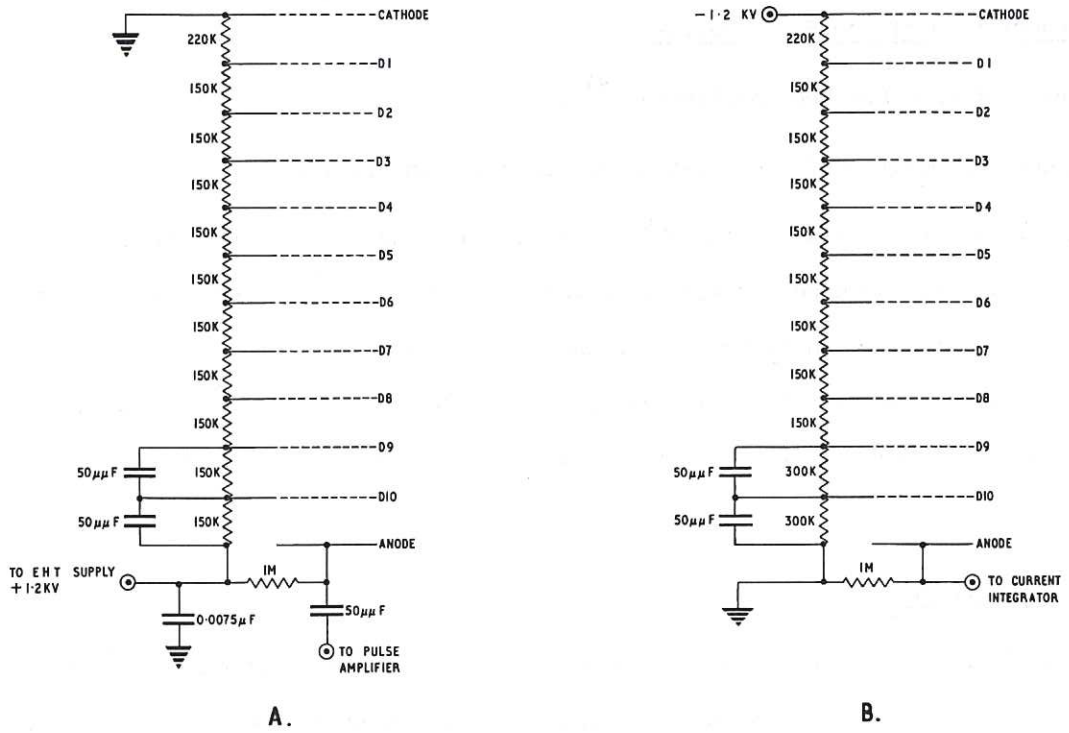

Fig. 15
The circuit used to define the dynode potentials of the photo-multiplier; A for detection of individual pulses and B for current integration

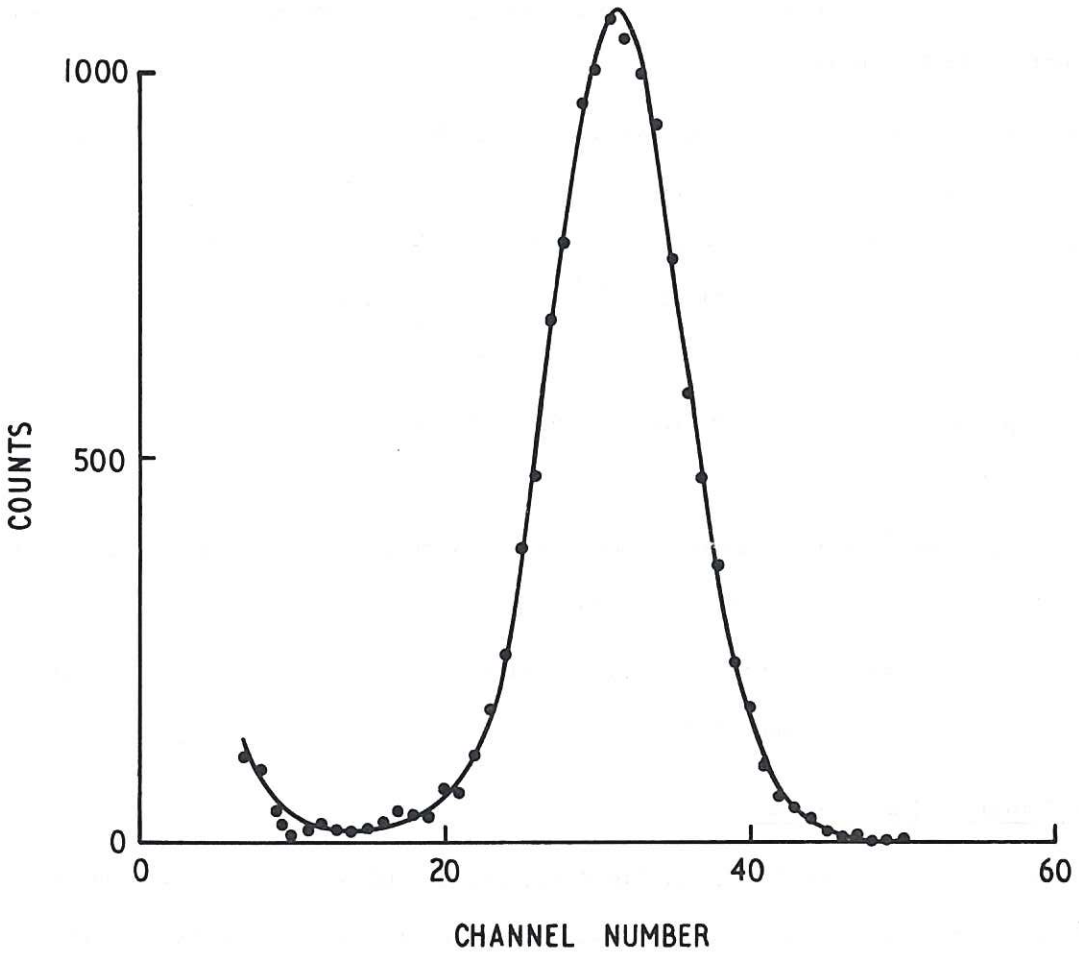

Fig. 16
Pulse height analysis for H^+ obtained from 150 keV H_3^+

individual pulses, the circuit can also be used to amplify the total beam current. In this case calibration is difficult, because the light output of the CsI crystal is not constant, but the current was only used for relative measurements. The inconstancy of the light output may conceivably be due to oil or carbon deposition on the crystal surface. To integrate the total current, the photomultiplier current was fed to a 108 μF capacitor whose charge was measured with a high impedance electrometer (Vibron). A typical amplified and integrated H_2^+ current charged the condenser to 1 volt in 100 sec. The estimated error in the uncalibrated Vibron reading was 3%.

3.6 Coincidence Technique

As was shown in 1.5 the expected dissociated fraction of H_2^+ due to the field is of the order of 10^{-5}. However a fraction $n \sigma \ell$ is dissociated in collisions with residual gas molecules; the density of the residual gas, n, is $10^{11}/cm^3$ for a pressure of 3×10^{-6} Torr; σ, the total cross-section for dissociation, is 2×10^{-16} cm^2 for 350 keV H_2^+ on O_2 and N_2[31], the distance ℓ between the 10^0 and 38^0 magnet is 80 cm. This, therefore, gives a contribution of the dissociation due to the residual gas, of 2×10^{-3}. Thus, in order to measure the field dissociation to the required accuracy, this contribution must be reduced. This can be achieved partly by measuring coincidences between H^0 and H^+. This eliminates the contribution due to $H_2^+ \rightarrow 2H^+$, $H_2^+ \rightarrow 2H^0$ and $H_2^+ \rightarrow H_2^0$ which together have about the same probability as $H_2^+ \rightarrow H^+ + H^0$. Moreover, the dissociation occurring between the 10^0 magnet and the electrodes (distance 30 cm) is also greatly eliminated because the dissociation products have an angular spread. This spread can be estimated by considering the collisions which result in dissociation as an electronic excitation into a repulsive state. The lowest of these states ($2P\ \sigma_u$) has an energy about 0.5 a.u. higher than the dissociation limit at, say, R = 2 a.u. (see Tables I and II). This results in an extra energy of 0.5×27 eV = 13.5 eV. If the original particle had an energy of 270 keV, the velocity ratio, that means the angular spread is $(13.5/270000)^{\frac{1}{2}} = 0.007$. Since the aperture in the first electrode is 0.1 mm, it is very improbable that both dissociation products will pass through.

A third background contribution which is eliminated by the coincidence technique is that due to dissociation on the edge of the 0.1 mm aperture, since this reaction is also likely to result in an angular spread. A further advantage of using coincidences is the elimination of background counts due to cosmic rays.

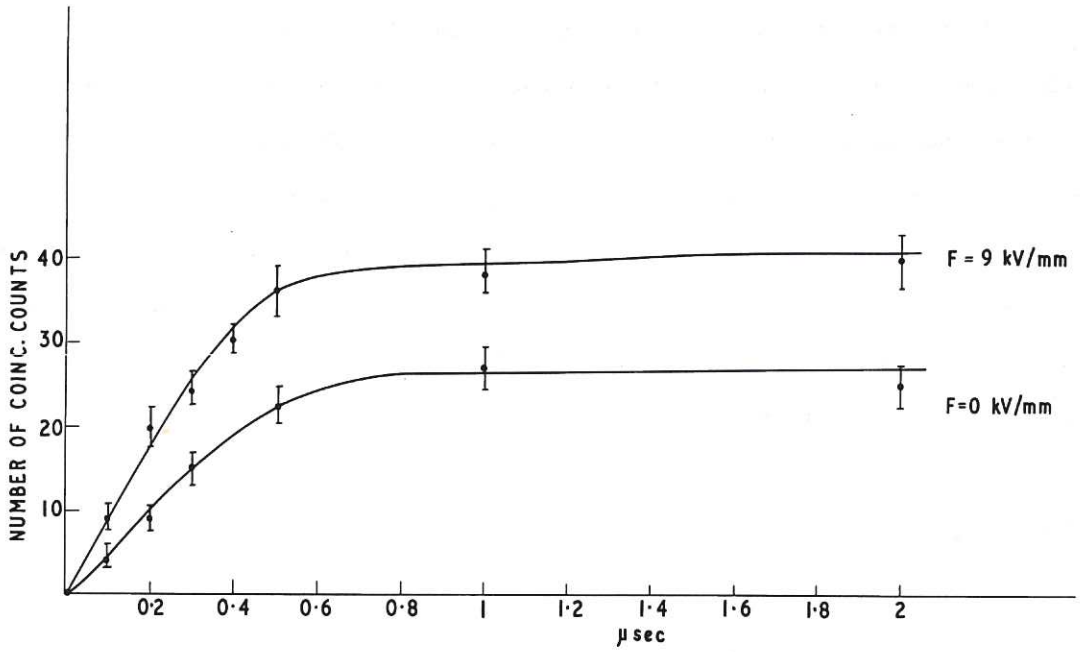

Fig. 17
The number of counts with the statistical error as a function of the coincidence time

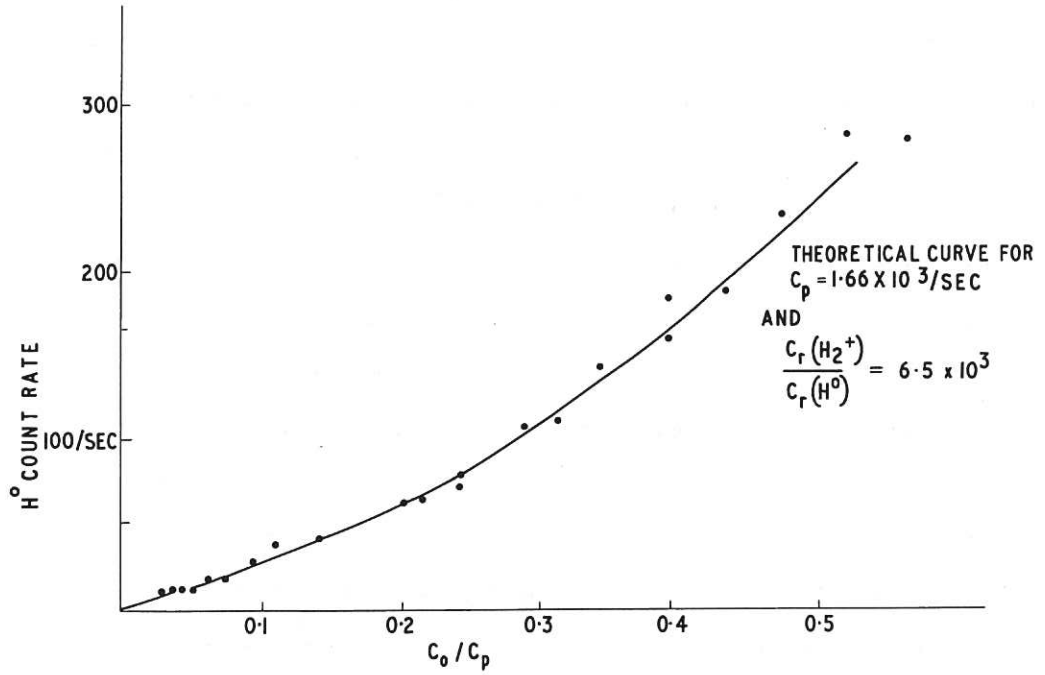

Fig. 18
The H° count rate as a function of the observed H_2^+ count rate. The H° count rate can be considered as proportional to the real H_2^+ count rate

The total observed reduction (see 3.10) in the H^0 and H^+ count rate, when taking coincidence only, was roughly an order of magnitude.

The maximum interval within which two pulses had to arrive to be considered as coincident (coincidence time) was determined experimentally to be 1 μsec (see Fig.17). If this interval were chosen too short, counts due to the same H_2^+ particle might be missed, if it were too long the contribution due to random coincidences would be large.

3.7 Correction for Dead Time

The pulses from the photomultipliers were amplified and discriminated. The pulses were about 5 μsec long. The actual dead time was measured as 6 μsec by applying a sine wave from a generator; those pulses were counted correctly up to 166 kc/s, no count being registered above this value.

This dead time therefore results in a maximum possible count rate $C_p = 1.7 \times 10^5$/sec. An observed count rate C_o of random pulses therefore requires a correction in order to arrive at the real count rate C_r. After each count the scaler is dead for $1/C_p$ sec. The integral dead time per sec is, therefore, C_o/C_p. The number of pulses per sec not counted thus is $C_r\, C_o/C_p$. Hence

$$C_r = C_o + C_r\, C_o/C_p \quad \text{or} \quad C_r = C_o/(1 - C_o/C_p) \qquad \ldots (5)$$

This equation holds only if the pulses are random which, however, was not the case in practice, since the beam intensity fluctuated. This was a result of variation in the accelerating potential induced by spurious charges on the belt driving the generator of the ion source power supply.

We therefore checked equation (5) by measuring the H^0 count rate. Since the pressure could be assumed to be constant, the H^0 count rate was a measure of the real H_2^+ count rate.

It can be concluded from the observation (see Fig.18) that equation (5) is applicable up to $C_o/C_p = 0.5$.

3.8 Verification of Beam Alignment

To verify that the detection covered the entire beam cross-section and to select the correct magnetic field for the 38^0 magnet, each detector was scanned by a slit; also, the

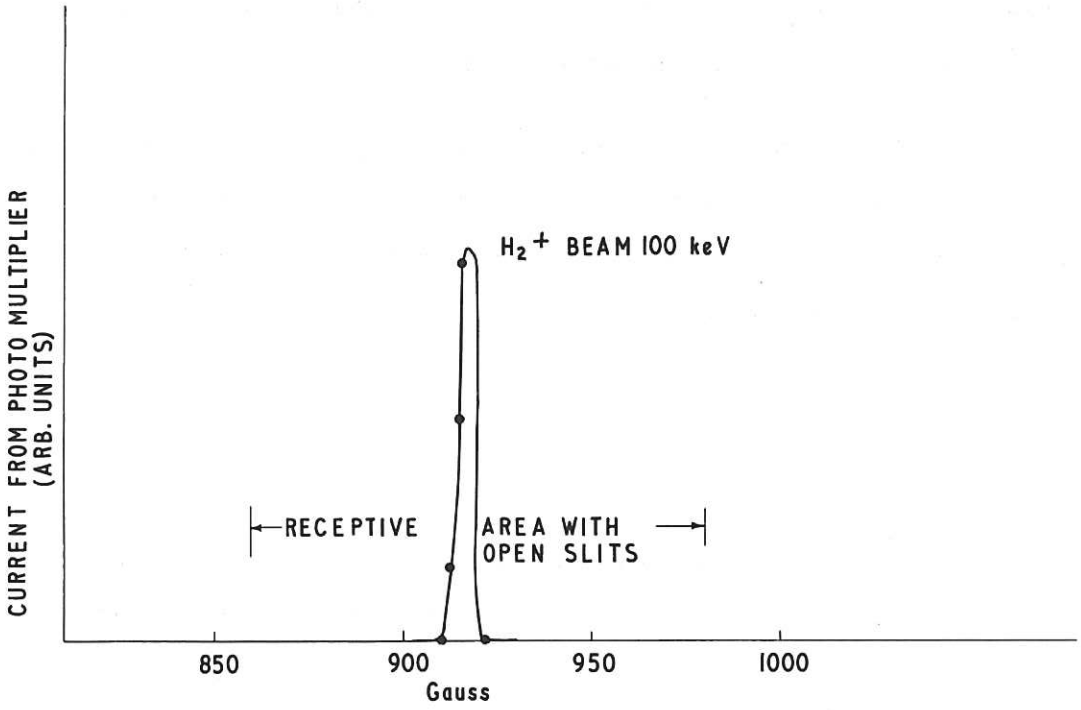

Fig. 19
Beam size compared with receptive area of detector

magnetic field was varied and the slit kept in a fixed position. These checks confirmed that the beam was much smaller than the exposed crystal area (see Fig. 19).

3.9 Time Necessary for Relative and Absolute Measurements

In relative measurement the current from the H_2^+ detector is fed into a 108 μF capacitor until the latter is charged up to, say, 1 volt. This makes possible the use of a higher H_2^+ beam than could be counted.

For the same given integral H_2^+ current, let A and B be the coincidence counts with and without voltage at the electrodes respectively. We now determine A - B as a function of the applied field. Since the statistical error on A and B is $\sqrt{A}$ and $\sqrt{B}$, the total error is $(A + B)^{\frac{1}{2}}$. The relative error is thus $(A + B)^{\frac{1}{2}}/(A - B)$. Now B, the coincidence count due to dissociation on the residual gas is $n \sigma \ell N_{H_2^+}$. For $n = 10^{11}/cm^3$; $\sigma = 10^{-16}$ cm^2; ℓ the distance between the electrodes and the 38^0 magnet is 14 cm; this gives $n\sigma\ell = 1.4 \times 10^{-4}$. The dissociated fraction by the field is of the order 10^{-5}. To measure this fraction with a 10% accuracy we find from

$$(A + B)^{\frac{1}{2}}/(A - B) = \left\{ \left[(10^{-5} + 1.4 \times 10^{-4}) + 1.4 \times 10^{-4} \right] N_{H_2^+} \right\}^{\frac{1}{2}} / (10^{-5} N_{H_2^+}) = \frac{1}{10}$$

that $N_{H_2^+}$, the number of H_2^+ ions, must be 3×10^8. To record this number with a count rate of 10^5/sec takes therefore about one hour for each field value.

For the relative measurement, instead of counting, the integral H_2^+ current is measured and the time necessary for the measurement is determined by the dead time of the coincidence

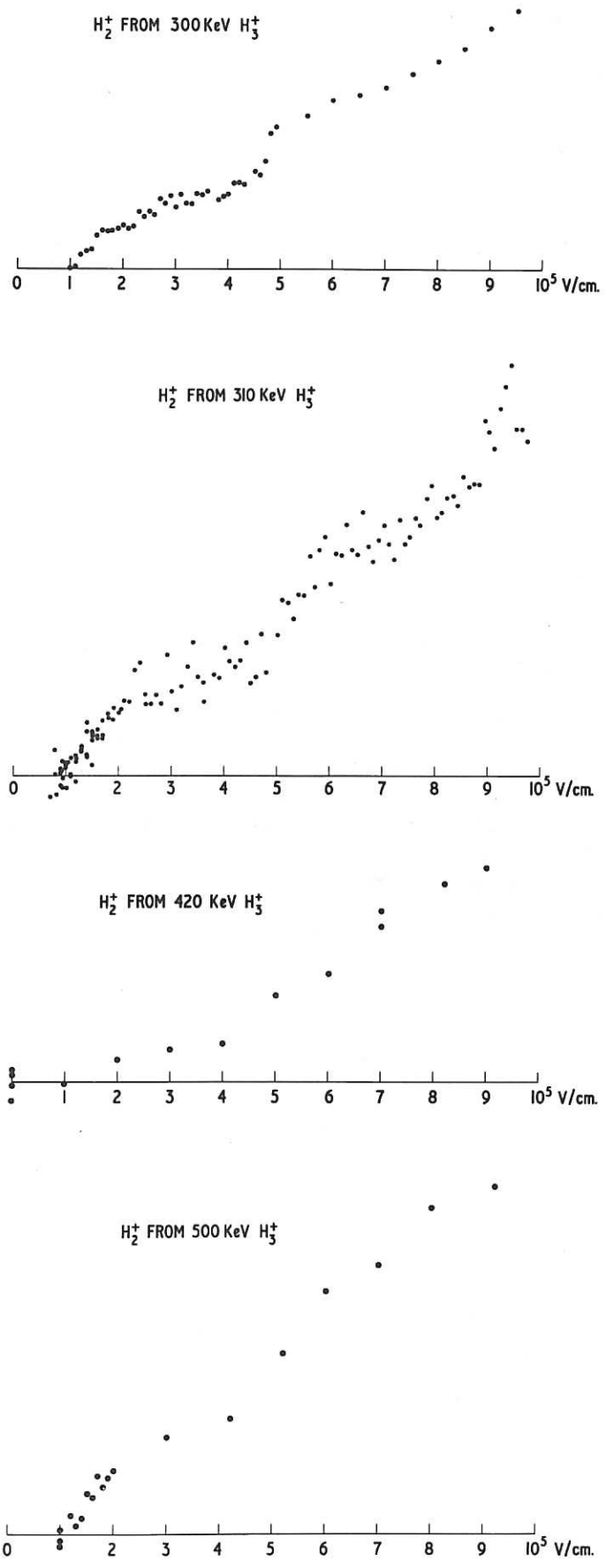

Fig. 20
The results of relative measurements. The ordinates, in relative units are proportional to the fraction of the H_2^+ beam dissociated

unit. For a count rate of 10^4/sec, a relative measurement would thus take $(1.4 \times 10^{-4} \times 3 \times 10^8)/10^4 = 4$ sec per field value.

3.10 Results of Measurements

For the relative measurements the ratio of the H^0, H^+ coincidence count rate to the H_2^+ current was measured with and without applying a voltage on the electrodes, and the changes in this ratio were determined as a function of the applied field. Some of the results are shown in Fig. 20. As can be seen the error is too large for individual levels to be observed.

Table IV gives a typical example of data obtained from H_2^+ formed by the break-up of 400 keV H_3^+, a gas target pressure of 2.5×10^{-3} Torr, a magnetic field of the 90^o magnet of 4.6 kG, of the 10^o magnet of 0.615 kG and the 38^o magnet of 2.32 kG and an electrode gap of 1 mm. The pressure in the electrode region was 2×10^{-6} Torr.

TABLE IV

Typical example of data: voltage applied on electrodes (in kV), integrated H_2^+ current (arb. units), H^0 and H^+ counts, and (H^0, H^+) coincidence counts. Each line corresponds to the field 10 sec. off and 10 sec. on.

V	H_2^+	H^0	H^+	COIN	V	H_2^+	H^0	H^+	COIN
0.0	0.535	31478	40159	2376	3.9	0.530	32191	39978	3219
0.0	0.530	31358	39851	2282	3.9	0.530	32960	40549	3244
0.0	0.535	31751	40251	2363	3.9	0.530	32389	39872	3218
0.0	0.535	31595	40089	2411	4.0	0.535	32784	39937	3326
0.0	0.535	31750	40069	2369	4.0	0.535	32341	40025	3327
0.0	0.540	31781	40426	2311	4.0	0.535	32797	40196	3264
0.0	0.540	32117	40682	2319	4.1	0.540	32310	40621	3336
0.0	0.535	31820	40579	2321	4.1	0.530	32809	40625	3331
0.0	0.540	31905	40756	2289	4.1	0.535	32613	40668	3320
0.0	0.540	31644	40705	2359	4.2	0.530	32754	40143	3167
0.0	0.530	31616	40721	2201	4.2	0.525	32241	40429	3177
0.0	0.530	31666	40160	2369	4.2	0.520	32214	40272	3319
0.0	0.530	31572	40022	2275	4.3	0.520	32208	40260	3329
0.0	0.530	31018	39872	2359	4.3	0.520	31880	39996	3254
0.0	0.520	31135	39202	2281	4.3	0.520	31899	39955	3296

The zero in the first column refers to no voltage being applied to the electrodes. Column 2 gives the Vibron reading in volts and is proportional to the integrated H_2^+ current. Column 3 gives the number of neutral counts N_{H^0}. Column 4 the number of proton counts N_{H^+} and column 5 the number of coincidences N_c. Columns 7 to 10 give the same values when a voltage according to column 6 (in kilovolts) is applied. These measurements were taken every ten seconds with the field alternatingly on and off.

Table V gives the results of processing these particular data. The first column gives the applied voltage in kV. The number of random coincidences in 10 sec is $N_{H^+} \times N_{H^0} \times 10^7$ because the coincidence time was 1 μsec.

TABLE V

Results of processing the particular data given in Table IV. The theoretical error derived from the statistical fluctuations in the count rate is up to three times smaller than the actual fluctuations in three successive observations

Voltage	Relative non-random coincidences	Difference	Average	Error (exp)	Error (theor)
0	4204.8				
3.900	5830.8	1625.9			
0	4069.9				
3.900	5868.6	1798.7			
0	4177.9				
3.900	5828.0	1650.1	1691.6	76.39	43.07
0	4269.8				
4.000	5972.1	1702.3			
0	4190.2				
4.000	5976.7	1786.5			
0	4041.7				
4.000	5854.5	1812.8	1767.2	47.13	43.59
0	4052				
4.100	5934.7	1882.2			
0	4097.0				
4.100	6033.4	1936.4			
0	3998.1				
4.100	5957.7	1959.6	1926.1	32.42	43.35
0	4130.0				
4.200	5727.4	1597.4			
0	3909.9				
4.200	5803.1	1893.2			
0	4232.1				
4.200	6133.2	1901.1	1797.2	141.33	42.93
0	4054.0				
4.300	6152.6	2098.5			
0	4217.6				
4.300	6012.5	1794.9			
0	4151.2				
4.300	6093.4	1942.1	1945.2	123.97	43.19

As can be seen, this gives a correction to the coincidence count rate of about 5%. The second column of Table V gives the ratio of the corrected number of coincidences and the integrated H_2^+ current. Column 3 gives the difference without and with field, column 4 the average of three measurements and column 5 the probable error, being the root mean

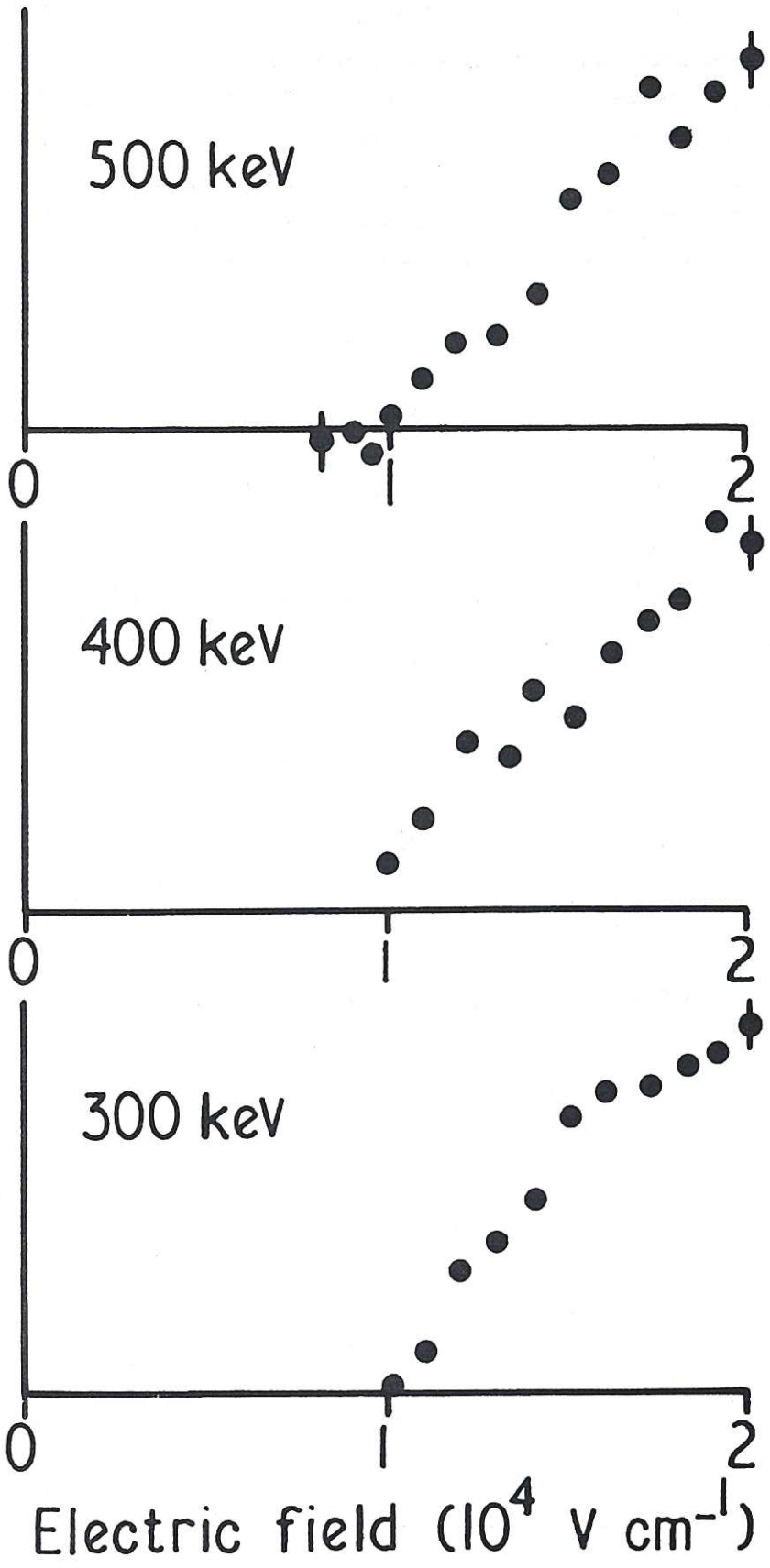

Fig. 21
Dissociation of H_2^+ ion beam near threshold for primary H_3^+ beam energies of 300, 400 and 500 keV

square of the three values. The last column gives the theoretical error based on statistical fluctuations as given in 3.9. It can be seen that the experimental error is up to 3 times higher than the theoretical one.

The conclusion which can be drawn from the results is the existence of a threshold at $0.96 \pm 0.05 \times 10^4$ V/cm (see Fig.21).

At 9.00×10^4 V/cm an absolute measurement was made by taking H_2^+ counts during 1000 sec for various energies. The results, presented in Table VI, give a fraction $1.6 \pm 0.2 \times 10^{-4}$ independent of the energy.

This agrees with Hiskes' theoretical value of 1.4×10^{-4} although this calculation was made for the case of H_2^+ being formed by electron impact on H_2 rather than from the break-up of H_3^+ .

TABLE VI

Results of absolute measurements at 9×10^4 V/cm. Each measurement is the result of counting both (H^0, H^+) coincidences and H_2^+ during 1000 sec

Energy of H_3^+	Fraction of H_2^+ dissociated at 9×10^4 V/cm
500 keV	1.9×10^{-4}
400 keV	1.6×10^{-4}
350 keV	1.6×10^{-4}
300 keV	1.4×10^{-4}
250 keV	1.5×10^{-4}
200 keV	1.4×10^{-4}

4. MEASUREMENT OF THE DIFFERENTIAL FIELD DISSOCIATION

4.1 Advantages of the second device compared with the first

In the measurements discussed in Chapter 3, the quantity measured was the integral field dissociation at the applied field.

In the experimental arrangement discussed in this chapter a field, gradually increasing in space, is applied perpendicularly to the direction of the H_2^+ beam. The deflection of the dissociation products then is a measure of the field at which the dissociation occurred (see Fig. 22). This provides a means of measuring the differential field dissociation with a relative accuracy sufficient to permit resolution of individual vibrational states.

4.2 Description of apparatus

The H_2^+ ion beam is defined by slits both before and after the 10^o magnet to a width of 0.2 mm and a height of 20 mm.

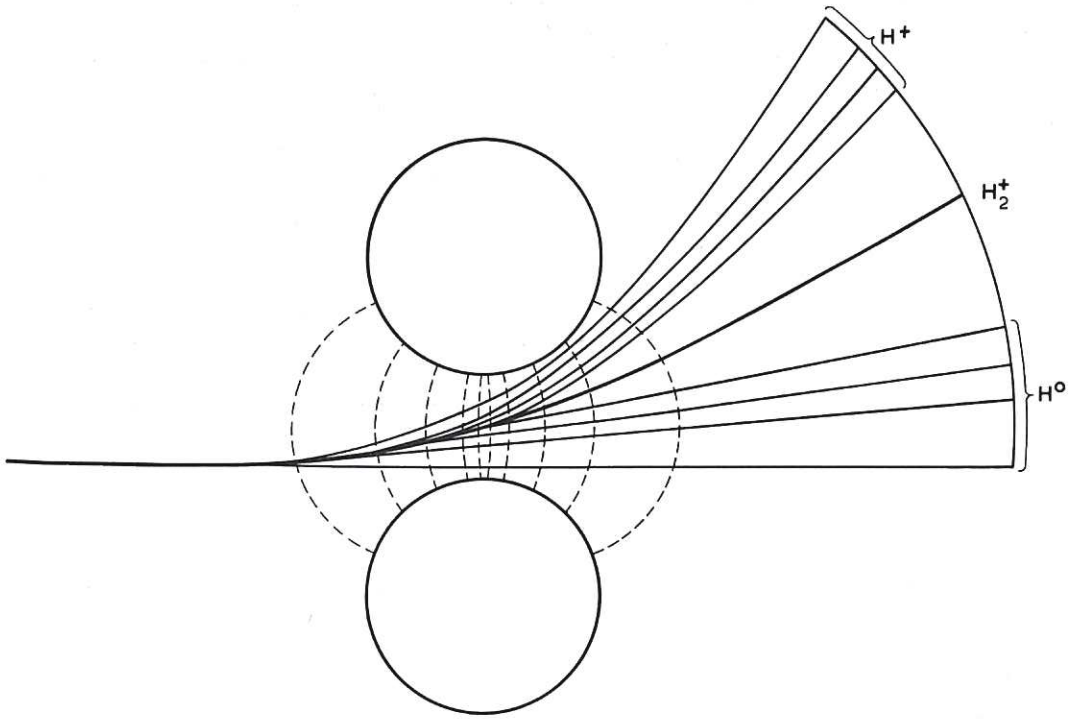

Fig. 22
The field produced by the cylindrical electrodes and trajectories of H_2^+ and its dissociation products for dissociation at various field strength. The deflection of either H^o or H^+ is a measure for the field at which dissociation occurred. This figure is not drawn to scale

The electric field is produced by two cylindrical electrodes of 24 mm diameter, a length of 50 mm and a variable gap of about 1 mm. The electrode axes are vertical, and thus perpendicular to the direction of the ion beam.

The H^0 and H^+ can be detected either with a photomultiplier detector or on a photographic film. The photomultiplier detector with CsI crystal is mounted on an arm rotatable about the centre of the field region at a radius of 30 cm. Particles emerging from the field region through any angle from -10^0 to 85^0 can be detected. The detector has a 0.5 mm slit in front of the CsI crystal. The resistor chain to define the dynode potentials is mounted on the valve base inside the vacuum.

The position of the arm is determined by means of a variable resistor attached to the arm. The photomultiplier current and a voltage proportional to this variable resistor were fed into an x - y recorder.

To register the H^0 and H^+ on photographic film, the photomultiplier detector can be swung out of the way. The film, standard Ilford HP3 35 mm, is mounted in an 85^0 arc about the centre of the electric field region at a radius of 47 cm. Some 10 m of film, corresponding to a dozen exposures, can be used without disturbing the vacuum.

To prevent the undissociated H_2^+ beam from charging up the film, which would produce breakdown patterns, a second moveable arm inside the vacuum holds a copper strip 5 mm wide which collects the undissociated H_2^+ current. This was also used as an indication of the beam current during the exposure of the film.

A typical H_2^+ current which, however, includes secondary electrons, was 3×10^{-10} A (measured as 3 mV over 10 MΩ).

4.3 The field of the cylindrical electrodes

To solve the potential problem of two infinitely long cylinders of radius R, separation d and a potential difference V_0, we first consider the field of two charged lines in the z-direction at $x = \pm a$; $y = 0$. Let the charges on the lines be $\pm$ Q/meter. The potential then is

$$V(x,y) = \frac{Q}{4\pi\varepsilon} \ln \frac{(a + x)^2 + y^2}{(a - x)^2 + y^2}$$

It can now readily be deduced that the equipotentials are cylinders and, by replacing two equipotentials by the cylinders in our potential problem, we can express Q and a in

terms of V_o, R and d. We then arrive at

$$V(x,y) = \frac{V_o \ln \frac{(a+x)^2 + y^2}{(a-x)^2 + y^2}}{4 \ln \frac{a + d/2}{a - d/2}}$$

in which

$$a = \sqrt{Rd + d^2/4}.$$

From this we derive

$$F_x = \frac{\partial V}{\partial x} = \frac{V_o}{2 \ln \frac{a + d/2}{a - d/2}} \left\{ \frac{a + x}{(a+x)^2 + y^2} + \frac{a - x}{(a-x)^2 + y^2} \right\}$$

The maximum field on the y-axis is

$$F(o,o) = \frac{V_o}{a \ln \frac{a + d/2}{a - d/2}} \equiv F_{max} .$$

For $d \ll R$ this becomes

$$F_{max} = V_o/d.$$

In order to calculate the deflection of H_2^+ and of the dissociation products, we now make the assumption that the y-component of the velocity is constant, which is the case if $V_o \ll E$, (the H_2^+ energy in eV). We further take for the field to which the particles are subjected

$$F = F_x\,(o,y)$$

We then find the deflection ψ of the undissociated H_2^+ which has an initial velocity in the positive y-direction

$$\operatorname{tg} \psi = \frac{v_\perp}{v} = \frac{\int_{-\infty}^{+\infty} e\, F_\perp \, dt}{[2eE/(2M+m)]^{\frac{1}{2}}} \simeq \frac{\int_{-\infty}^{+\infty} F_x(o,y)\, dy}{2E} \qquad \ldots (6)$$

$$= \frac{F_{max}\, a}{2E} \int_{-\infty}^{+\infty} \frac{a}{a^2 + y^2}\, dy = F_{max}\, a\, \pi/(2E)$$

For $F = 10^5$ V/cm, d = 1 mm, R = 12 mm and E = 300 keV we find $\operatorname{tg} \psi = 0.18$ which corresponds to 8.5 cm on the film.

We now consider the case where the H_2^+ dissociates at y_o corresponding to a field F_o. The resulting H^o is then deflected as follows

$$\frac{v_\perp}{v} = \frac{F_{max}\, a}{2E} \int_{-\infty}^{y_o} \frac{a}{a^2 + y^2}\, dy$$

$$= \frac{F_{max}\, a}{2E} \left(\operatorname{arctg} \frac{y_o}{a} + \frac{\pi}{2} \right)$$

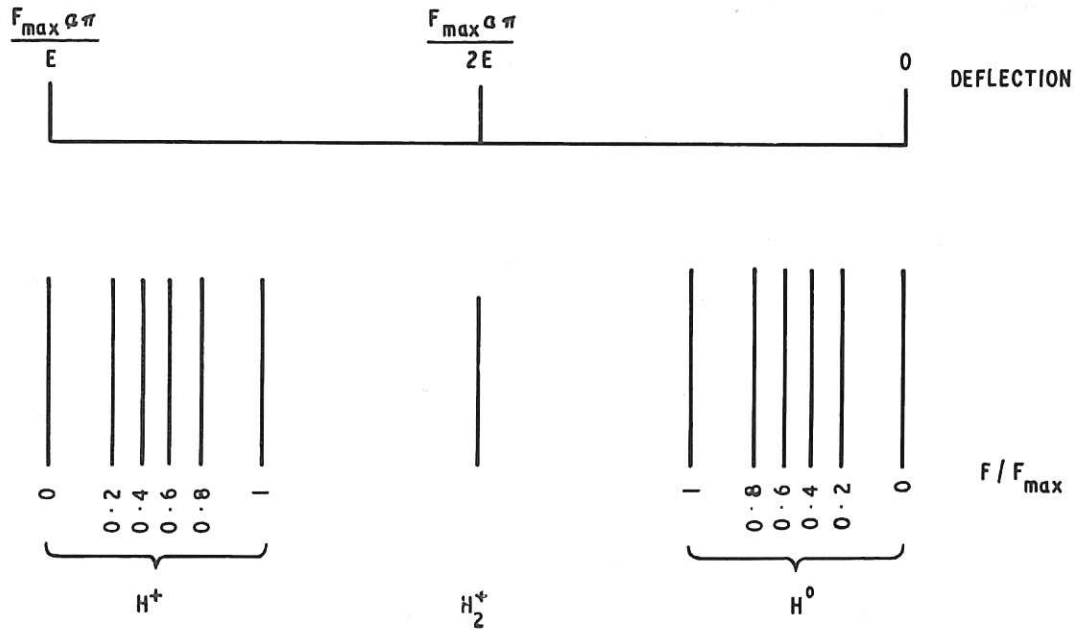

Fig. 23
Deflection of dissociation products as a function of the field at which they are produced. The deflection of the undissociated H_2^+ is also indicated

or since $F_o = F_{max} \frac{a^2}{a^2 + y_o^2}$ this can be written as

$$\frac{F_{max}\,a}{2E} \left(-\text{arctg} \left[\frac{F_{max}}{F_o} - 1 \right]^{\frac{1}{2}} + \frac{\pi}{2} \right)$$

The deflection of the resulting H^+ is

$$\frac{F_{max}\,a}{2E} \left\{ \int_{-\infty}^{y_o} \frac{a}{a^2+y^2}\,dy + 2 \int_{y_o}^{\infty} \frac{a}{a^2+y^2}\,dy \right\}$$

$$= \frac{F_{max}\,a}{2E} \left(3\pi/2 + \text{arctg} \left[F_{max}/F_o - 1 \right]^{\frac{1}{2}} \right)$$

Fig. 23 illustrates how the deflection of H^0 and H^+ depends on the field at which they are produced. The H^+ and H^0 signals are symmetrical about the position of the undissociated H_2^+.

In order to verify if the approximations made, were justified, numerical computations of the trajectories were carried out for the exact field of two infinitely cylindrical electrodes.

The agreement was better than 3% for all practical parameters.

We found for instance for

$$E = 400 \text{ keV}$$
$$V = 10 \text{ kV}$$
$$d = 0.8 \text{ mm}$$
$$R = 12$$

a deflection

$$\frac{x}{y} = 0.156$$

and

$$\frac{v_x}{v_y} = 0.157$$

whereas

$$\frac{Va\pi}{2dE} = 0.153$$

In measuring the deflection and applying equation (6) we found an agreement to within 5 per cent, which is the error in the measurement of the separation d.

4.4 Maximum Attainable Field

The maximum obtainable field is limited by the condition that both the H^0 and the H^+ formed at low fields must pass through the electrode gap (see Fig.22). The separation between H^0 and H^+ produced at a distance L from the electrodes ($L \gg a$) is given by

$$\Delta x = \int_{-L}^{0} v_x \, dt \simeq \frac{1}{v} \int_{-L}^{0} v_x \, dy \simeq \frac{1}{v} \int_{-L}^{0} \frac{1}{M} \left(\int_{-L}^{y} e F_x \, dt \right) dy$$

$$\simeq \frac{eF_{max}}{Mv^2} \int_{-L}^{0} \left\{ \int_{-L}^{y} \frac{a^2}{a^2+y^2} \, dy \right\} dy \simeq \frac{F_{max}}{E} \int_{-L}^{0} \left\{ \text{arc tg}(y/a) + \pi/2 \right\} dy$$

$$= \frac{F_{max} a}{E} \left\{ y \text{ arc tg}(y/a) - \tfrac{1}{2} a \ln \left[1 + (y/a)^2 \right] + \tfrac{1}{2} \pi y \right\} \Bigg|_{-L}^{0}$$

$$\approx \frac{F_{max} \, a^2}{E} \ln (L/a) \qquad \ldots (7)$$

The approximations made were checked against numerical computations of trajectories. The agreement was better than 3%.

In the limiting case that $\Delta x = d$, the maximum field, according to (7) is

$$F^*_{max} = \frac{Ed}{a^2 \ln(L/a)} \simeq \frac{2E}{R \ln(L^2/Rd)} \qquad \ldots (8)$$

for

$$\left.\begin{array}{l} E = 300 \text{ keV} \\ d = 1 \text{ mm} \\ R = 12 \text{ mm} \end{array}\right\} \rightarrow a = 3.5 \text{ mm}$$
$$L = 7 \text{ cm}$$

this gives

$$F^*_{max} = 8.1 \times 10^4 \text{ V/cm.}$$

The maximum possible deflection of H^+ is

$$\operatorname{tg} \psi = \frac{F^*_{max}\ a\ 2\pi}{2E} = \frac{d\ \pi}{a\ \ln(L/a)}$$

which is a purely geometrical factor. With the above dimensions we find $\operatorname{tg} \psi = 0.30$.

The real maximum field is still lower than F^*_{max} because of the finite width of the beam. If we had chosen a smaller value for R we could according to (8) have allowed a higher field. However, in that case either a smaller value of d would have been necessary, which has the disadvantage that the beam width must be reduced, or a higher value of V, which would cause breakdown.

On the other hand, when one of the H^0 or H^+ signals is lost, the other still carries the full information of the field dissociation, so that in this case the maximum field can be $2F^*_{max}$.

4.5 Time necessary for the measurements

The H_2^+ current available is of the order 10^{-10} Amp.

For measurements with the moveable detector we require, say, 10^4 particles per sec in the 0.5 mm detector slit. Since the radius of curvature is 30 cm, this corresponds to 0.002 radian; the region of interest is 0.2 radian. When we further estimate that a fraction 10^{-4} of the H_2^+ beam is dissociated, we find a recording time of

$$t = \frac{0.2}{0.002} \quad \frac{10^4}{8.10^8 \times 10^{-4}} \simeq 10 \text{ sec.}$$

The disadvantage of this approach lies in the fact that the H_2^+ beam intensity fluctuates. We therefore either have to take the average of many recordings or, alternatively, plot the ratio of the photomultiplier current and the H_2^+ current. We did not apply this latter system since a suitable electronic divider was not available.

We used the signal from the detector mainly as an indication of the beam alignment (4.7) and for quick but inaccurate measurements.

To estimate the exposure time required for a measurement on photographic film, we make the following assumptions.

1. The resulting signal is recorded on 20 cm^2 film.
2. Each particle activates 1 μ^2, corresponding to one grain.
3. 10% of the exposed film should be activated.

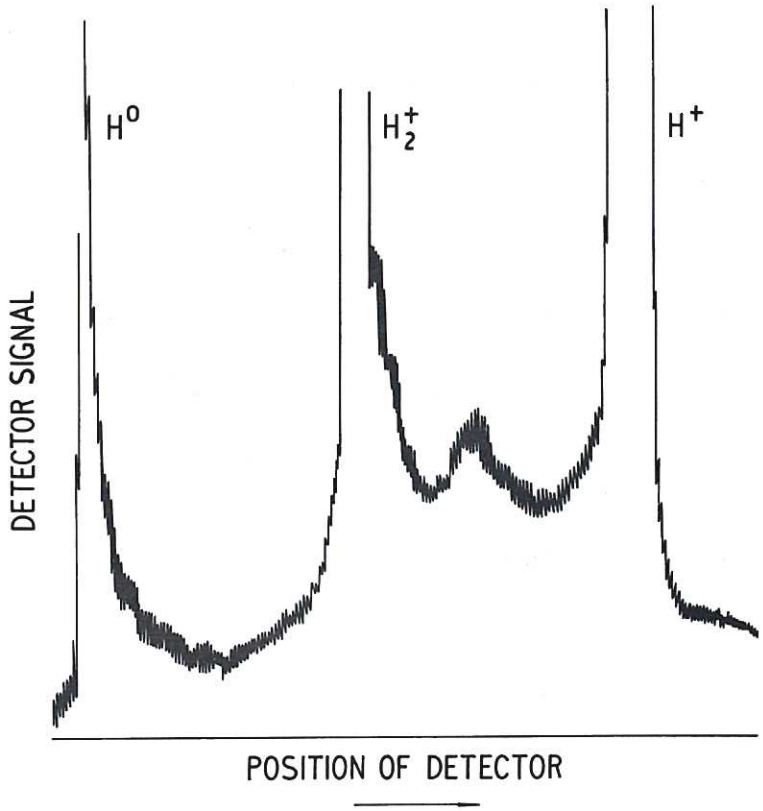

Fig. 24
The signal from the photomultiplier detector as a function of its position

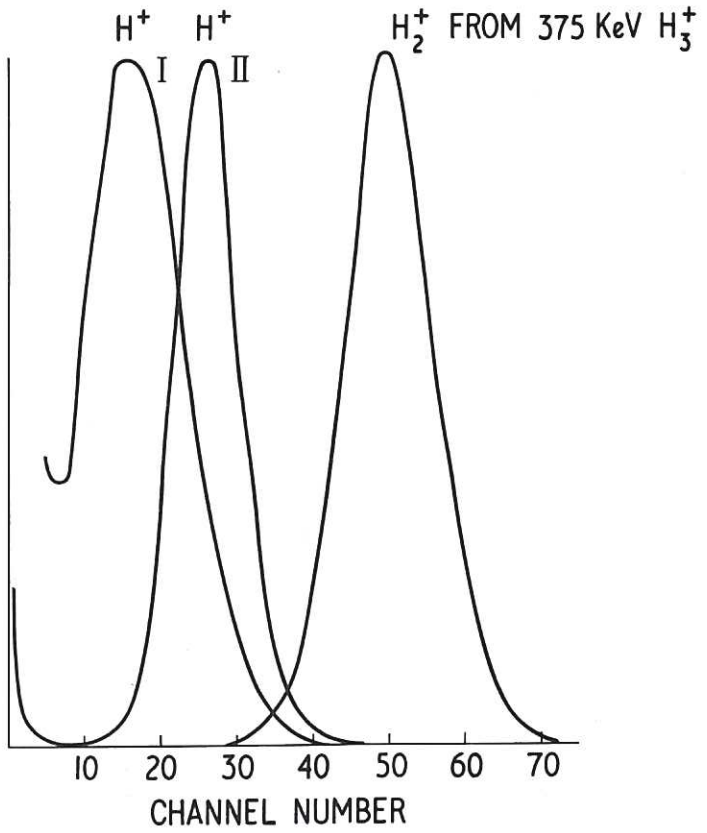

Fig. 25
Pulse height analysis of H^+ beam originating from high field region with and without alignment slits (I and II respectively)

We then arrive at an exposure time

$$t = \frac{20}{10 \times 10^{-8} \times 6.10^{8} \times 10^{-4}} = 3300 \text{ sec.}$$

We found in fact that one hour is a good exposure time when the H_2^+ current is measured as 10^{-10}A (this includes secondary electrons).

4.6 Results from the detector signal

In preliminary results a plot of the detector current versus position, gave signals of which Fig.24 gives an example. These indicated H^+ originating from the maximum field region. By pulse-height analysis it was shown that this signal was due to H_2^+ being scattered on the electrode system (see Fig.25). This effect was subsequently eliminated by proper beam alignment, and limiting slits. To do so the 0.2 mm x 20 mm slit after the 10^o magnet was first placed in such a position that the undeflected beam kept clear of the insulated electrode. The beam was then further limited by reducing the aperture of the slits before the 10^o magnet. The electric field was then switched on (by applying a positive potential to the insulated electrode) and the voltage on the electrodes determined, for which the H_2^+ beam intensity was appreciably reduced by collisions with the earthed electrode. The final voltage for the actual field dissociation measurement was then chosen well below this value. This fully eliminated the spurious signal from Fig.24, and pulse height analysis indicated clearly that no H_2^+ was scattered (see Fig.25).

When the pressure was sufficiently low ($< 10^{-6}$), two peaks in the recording of detector current versus position could be observed when a field of the order 10^5 V/cm was applied. We believe that these peaks result from field dissociation of the 19th and 18th vibrational level respectively (v = 18 and v = 17). However as a result of the beam fluctuations, these measurements were too inaccurate to determine the relative populations of these excited states.

When the detector was fixed in a position corresponding to the v = 18 level, its current was plotted as a function of the H_2^+ beam current. This produced a straight line while the beam intensity fluctuated. The slope of this line is a measure of the population of the excited state. We then varied some parameters to see whether this population could be changed.

We found no dependence on the following parameters:

1. Oscillator power of ion-source.
2. Extraction voltage of ion-source.

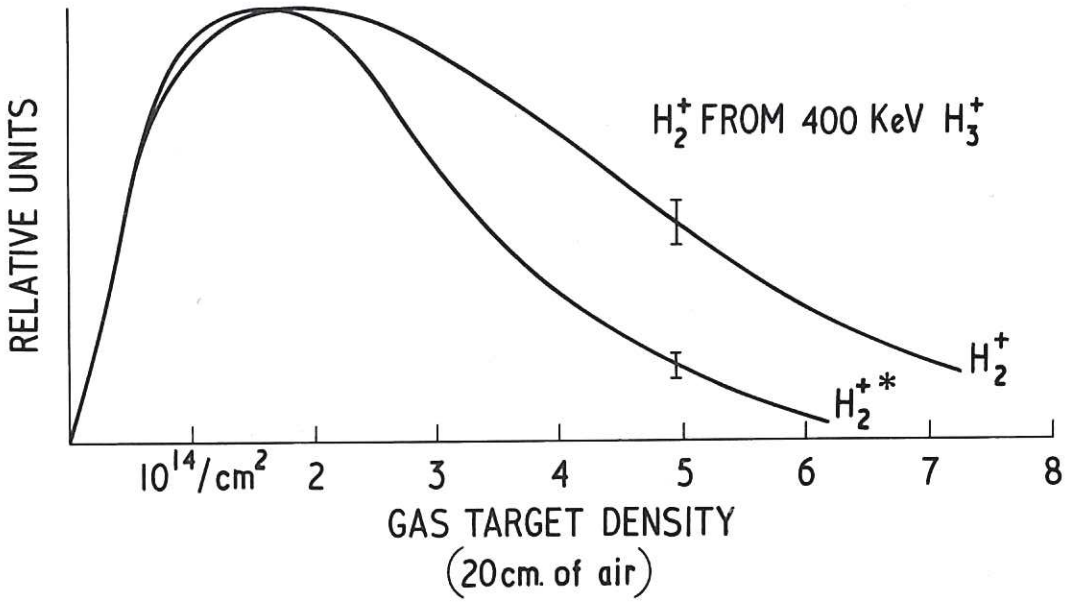

Fig. 26
The production of H_2^+ and H_2^{+*} from 400 keV H_3^+ as a function of gas target density. The ordinate is in relative units and linear scale

3. Acceleration voltage with a fixed 90^o and 10^o magnet current; this is therefore merely a variation in beam alignment.
4. Aperture of slits before 10^o magnet.
5. Pressure in ion source.

A variation of 10% in the ratio with a variation of the H_2^+ beam intensity by a factor 10 would have been observed.

We found however an observable effect of the gas target pressure in the sense that the excited state population decreases while the gas target pressure increases. This effect was even higher than the photomultiplier current indicated, since the latter also includes some 30% dissociation on the residual gas which increases with the gas target pressure. Fig. 26 gives the results. This confirms experiments by Sweetman[32] in which excited H_2^+ appears to have a slightly higher cross-section for dissociation than H_2^+ in the ground-state. It also means that the trapping in DCX-1 could be optimised by having a gas target pressure just below the one that produces maximum H_2^+ .

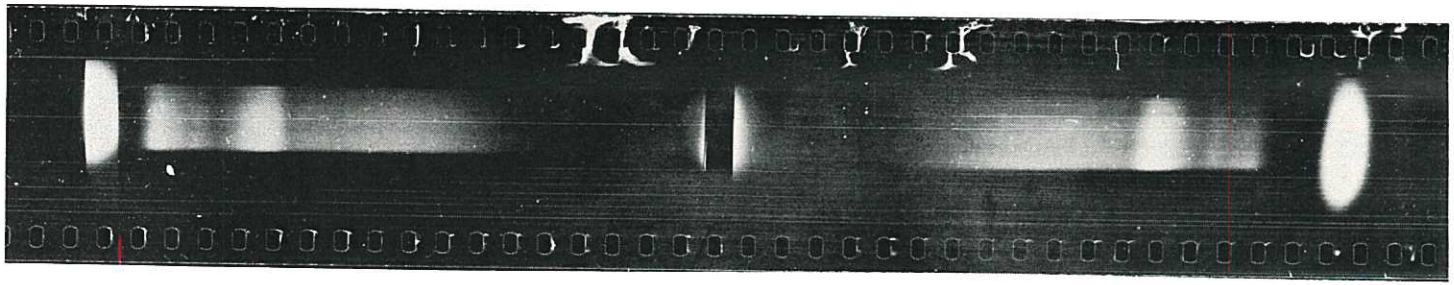

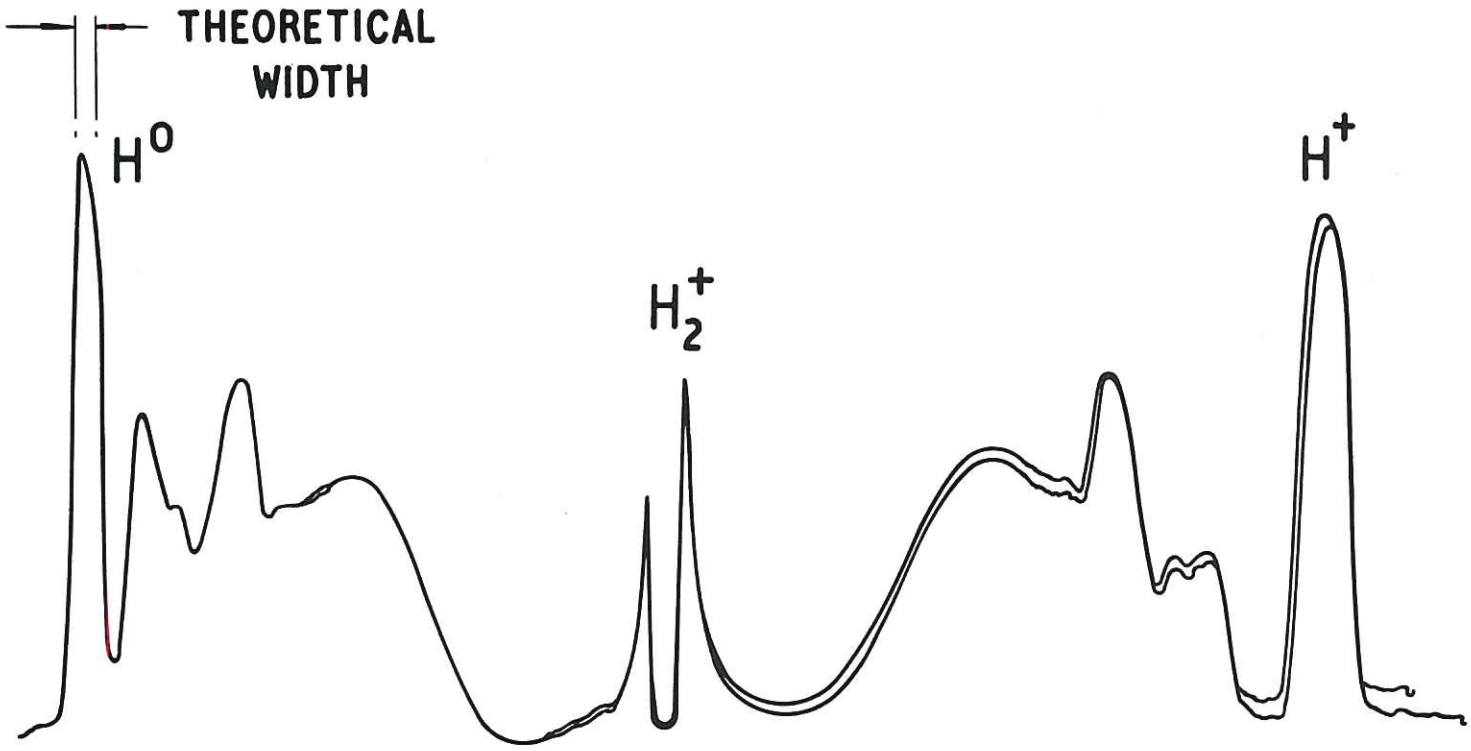

Fig. 27
An example of film exposure measurement and the result of photo densitometry of this example. The two high peaks are due to H^0 and H^+ produced at background gas collisions. The other signals are due to field dissociation. The undissociated H_2^+ is taken away to avoid damage of the film

4.7 Results of Photographic Measurements

The advantage of the photographic method compared with the moveable detector technique, is that dissociation at different fields is registered simultaneously. The final density distribution on the film is therefore independent of beam fluctuations, and a high accuracy in the determination of the relative populations is possible. We have not attempted to do absolute measurements since this would mean measuring the H_2^+ beam in a 5 mm wide Faraday cup, calibrating the film and relying on constant developing conditions, constant film quality etc. We assumed that the absolute measurement from 3.10, Table VI, is also applicable in the present case of a field perpendicular to the direction of the H_2^+ ion beam. The current of the undissociated H_2^+ was collected by the 5 mm copper strip and was fed into an 8 μF capacitor. The voltage of this capacitor was used as an indication of the integrated H_2^+ current. A typical charge of 1 μ Coulomb was collected during an exposure time of about an hour.

The film was developed by the normal process used for light exposures. A typical example of the film record is shown in Fig.27 which also gives the result of photodensitometry of this particular example. The two high peaks represent H^o and H^+ originating by dissociation on the background gas (see 4.8). The widths of these peaks can be estimated by the picture of the dissociation process as given in 3.6. We found there a typical angular spread of 7×10^{-3}. This corresponds to 3.3 mm on the film as indicated.

It can be seen that part of the H^+ beam is missed in this example. This can be explained by collisions with the electrodes since the condition $F_{max} < \frac{E\,d}{a^2 \ln (L/a)}$ (see 4.4) was not satisfied although the main H_2^+ beam kept clear of the electrodes.

To reduce the back-ground contribution a good vacuum was required. By having the film dried for about a week in a separate vacuum device and by pumping another 36 hours after the film was transferred to the experimental device, we were able to reach a pressure of 5×10^{-7} Torr with this 10 meter film in the vacuum. This reduced the background contribution $n\sigma\ell$ to about a fraction 3×10^{-6}, where ℓ is the length of the high field region, of order 1 mm.

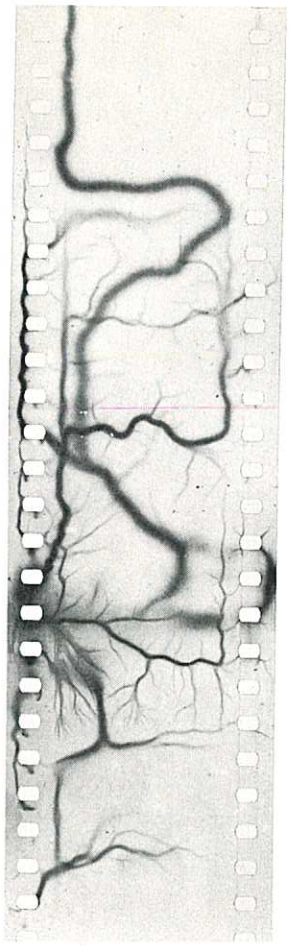

Fig. 28
Breakdown patterns produced on the extremely dry film when winding film is too fast

The film being completely dry, had to be handled very carefully. Firstly, because it was very brittle and, secondly, because of the hazard during winding of electrostatic charges being set up which might produce breakdown patterns (see Fig.28).

Another practical difficulty was vacuum breakdown between the electrodes. Although we could keep 28 kV over a 1 mm gap for a few minutes, even 10 kV often caused breakdown in the course of one hour's exposure. A safety device in the H.T. power supply then disconnected the H.T. and consequently the H_2^+ beam, no longer being deflected onto the collector, spoiled the exposure. This in fact occurred to some 70% of the 100 exposures taken.

4.8 Analysis of Photographic Results

Due to collisions with residual gas a fraction $n\sigma\Delta y$ is dissociated in a length Δy. A dissociation at $y = y_o$ causes a deflection of H^o given by

$$\operatorname{tg} \psi = \frac{F_{max}\, a}{2E} \left\{ \tfrac{1}{2}\pi - \operatorname{arctg} (y_o/a) \right\}$$

and, similarly, for H^+ by

$$\operatorname{tg} \psi = \frac{F_{max}\, a}{2E} \left\{ 3\pi/2 + \operatorname{arctg} (y_o/a) \right\}$$

An interval Δy corresponds to an interval $\Delta\psi = \Delta y \frac{\partial \psi}{\partial y}$, and we find a density distribution $D(\psi)$ due to residual gas collisions given by

$$\frac{N_{H_2^+}\, n(\sigma_1 + 2\sigma_2 + \sigma_3)}{2\, R_o\, E} \left\{ 1 + \operatorname{tg}^2(\tfrac{1}{2}\pi - \psi/\alpha) \right\} /cm^2$$

due to H^o, and

$$\frac{N_{H_2^+}\, n(\sigma_3 + 2\,\sigma_4)}{2\, R_o\, E} \left\{ 1 + \operatorname{tg}^2(3\pi/2 + \psi/\alpha) \right\} /cm^2$$

due to H^+,

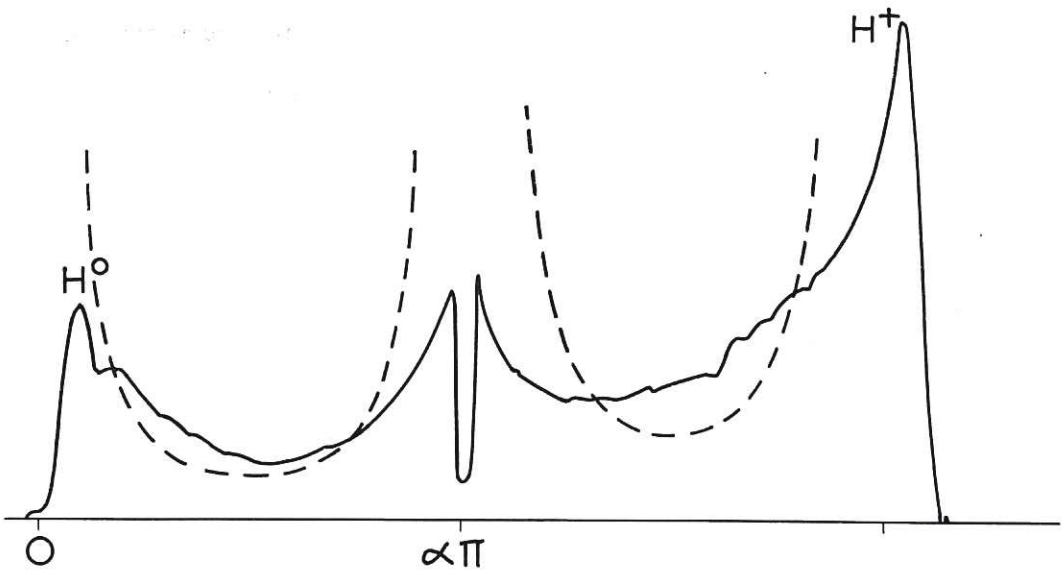

Fig. 29
The theoretical and experimental contribution due to collisions with residual gas

where $N_{H_2^+}$ is the number of H_2^+ particles,

$\alpha = \frac{F_{max}\, a}{2E}$,

σ_1 is the cross section for the reaction $H_2^+ \rightarrow H_2^o$,

σ_2 for $H_2^+ \rightarrow 2\ H^o$,

σ_3 for $H_2^+ \rightarrow H^o + H^+$,

σ_4 for $H_2^+ \rightarrow 2\ H^+$.

and R_o is the radius of curvature of the detector or the film.

Fig.29 illustrates the signal given by these expressions in relative units. The experimental signal, obtained by raising the background pressure, is also shown.

Since the contribution from background gas collisions is a minimum at the angle corresponding to the highest field, and because it is symmetrical about this minimum, it is easy to distinguish between the signal due to field dissociation and that of background gas collisions.

We have seen that the deflection of H^o, produced at a field F is given by

$$\operatorname{tg} \psi = \frac{F_{max}\, a}{2E} \left(\tfrac{1}{2}\pi - \operatorname{arctg} \left[F_{max}/F - 1 \right]^{\frac{1}{2}}\right) \qquad \ldots (9)$$

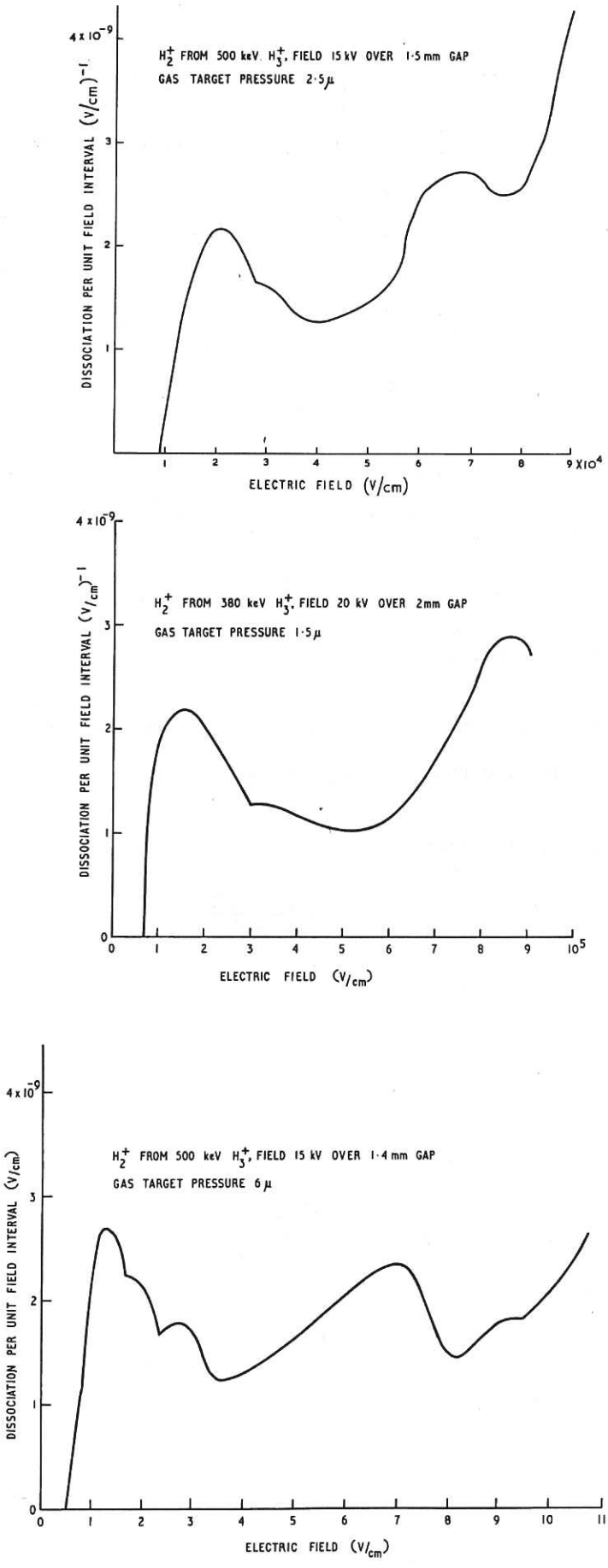

Fig. 30
The experimental results of differential field dissociation of H_2^+

A field interval ΔF corresponds to an interval $\Delta\psi$ given by

$$\Delta\psi = \frac{\partial\psi}{\partial F}\ \Delta F = \frac{a\Delta F}{2E}\left[(F/F_{max}) - (F/F_{max})^2\right]^{-\frac{1}{2}} \qquad \ldots (10)$$

The density distribution $D(\psi)$ on the film, after substracting the background, is therefore to be analysed as follows.

1. The deflection ψ is expressed in terms of F/F_{max} according to (9).
2. $D(\psi)$ is then multiplied by $\left[(F/F_{max}) - (F/F_{max})^2\right]^{\frac{1}{2}}$ according to (10)
3. The differential field dissociation curve $f(F)$ thus obtained is calibrated by

$$\int_0^{F=9\times10^4\ V/cm} f(F)\ dF = 1.6 \times 10^{-4}$$

according to table VI.

The results are shown in Fig.30.

If d is not measured directly, which would only be possible by taking out the electrode system, it can be derived from the H_2^+ deflection in the following way.

We eliminate d and a from (see 4.2)

$$F_{max} = V/(a \ln \frac{a + d/2}{a - d/2})$$

$$tg\ \psi = F_{max}\ a\pi/(2E)$$

and

$$a = (Rd + d^2/4)^{\frac{1}{2}}$$

This gives, when neglecting terms of order $(\frac{d}{R})^2$,

$$F_{max} = \frac{4E^2\ tg^2\psi}{R\ \pi^2\ V} - \frac{V}{6R}$$

The estimated errors are

$$\Delta E = 2\%$$

$$\Delta\ tg\ \psi = 3\%$$

$$\Delta R = 2\%$$

resulting in an error $\Delta F_{max} = 7.5\%$.

If d is measured directly with an accuracy of 5% the resulting error in F_{max} is also 5%.

5. COMPARISON BETWEEN THEORY AND EXPERIMENT

5.1 Threshold Experiment

In 3.10 we determined a threshold field of $0.96 \pm 0.05 \times 10^4$ V/cm, which was thought to be due to the $v = 18$, $J = 3$ levels. We have computed (2.4) that there are infact 3 levels which are above these namely 19, 0, 0; 19, 1, 0 and 19, 1, 1. However these are so weakly bound that the $\vec{v} \times \vec{B}$ field in the 10^0 magnet has undoubtedly fully removed. these states. The binding energy of 19, 0, 0 being 3.8×10^{-6} a field of 500 V/cm would be sufficient for dissociation according to the classical estimation given in 2.5. Inclusion of these levels in the measurements would require H_2^+ energies below 10 keV. This would have been difficult because of the problem of detection and because of the higher cross section for collisions on residual gas. We have therefore not attempted to measure these levels.

To compute the signal to be expected in the threshold experiment, we have approximated the field shape, as given in 3.4, by a parabolic one

$$F(x) = F_{max} \left[1 - \left(\frac{x}{0.75} \right)^2 \right]$$

where

$$F_{max} = \alpha \, V/d$$

and x is in mm.

This fits the field, as computed in 3.4, near its maximum.

The dissociated fraction is then given by

$$1 - \exp \left[- \frac{1}{v} \int_{-\infty}^{+\infty} P_t(F) \, d x \right]$$

where v is the velocity, which was taken to be 4.4×10^8 cm/sec corresponding to 300 keV H_3^+. P_t, the dissociation probability, was given in 2.5. We computed the above expression for the states $v = 18$; $J = 3$; $m = 0, 1, 2, 3$ for various values of F_{max}.

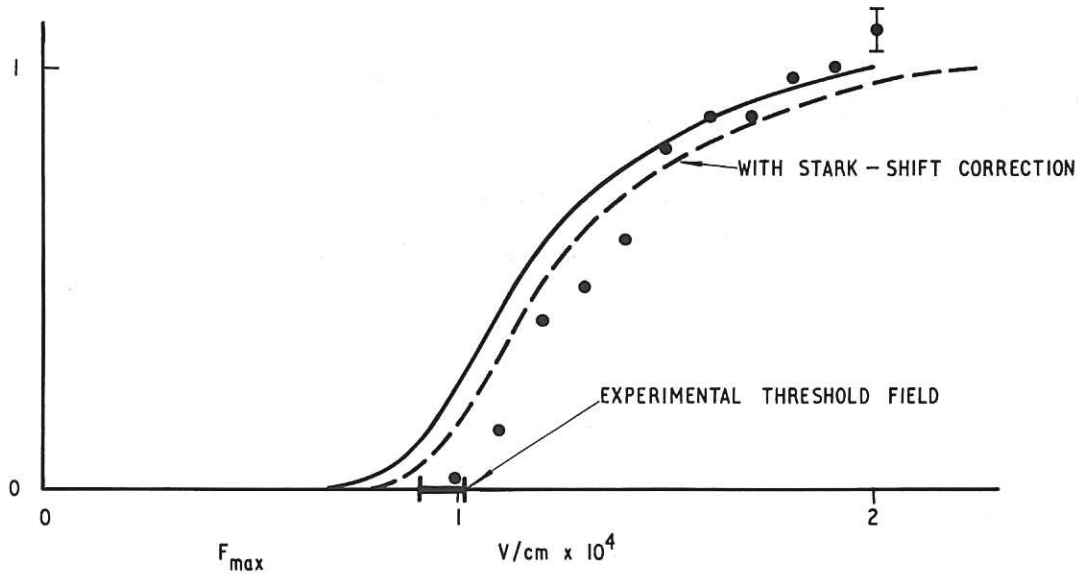

Fig. 31
Results of computations of dissociation probability of H_2^+ obtained from 400 keV H_3^+ in an electric field with a maximum F_{max} and decreasing parabolically to zero in 0.75 mm on either side. Experimental points are also indicated

We assumed that the seven substates, $m = -3 \ldots + 3$, are equally populated (the field dissociation depends on $|m|$ only). The results are given in Fig.31.

In 2.5 we have neglected the Stark shift of the energy levels. Hiskes estimated that this effect results in a 5–7% shift to higher fields for dissociation[33].

In Fig.31 we have also included a correction for this effect. We then arrive at a theoretical value of a 'threshold' of 0.93×10^4 V/cm. The agreement is therefore satisfactory.

5.2 Differential Field Dissociation Experiment

To compare the results of the differential field dissociation with the theory we have computed the case for which $F_{max} = 10^5$ V/cm; $d = 1$ mm and used the detailed field shape given by $F = F_{max} \frac{a^2}{a^2+y^2}$.

The dissociation probability of a level with a population Pop in a field interval ΔF is given by

$$-\Delta \text{ Pop} = \text{Pop} \left\{ 1 - \exp \left[- \Delta t P_t(F) \right] \right\}$$

in which Δt is the time spent in the field interval.

For the velocity v we took 5×10^8 cm/sec corresponding to 400 keV H_3^+.

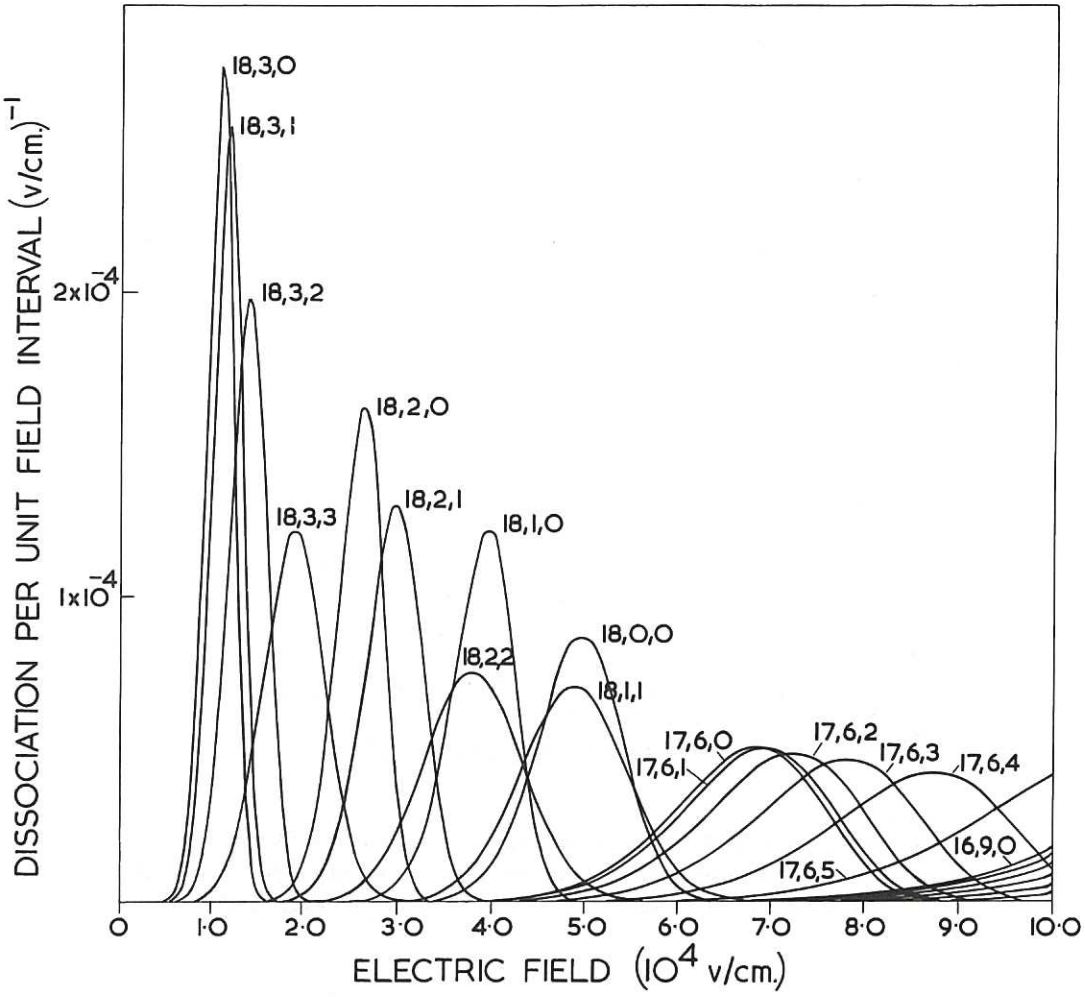

Fig. 32(a)
Dissociation probability of various levels in a field $F = F_{max}\ a^2/(a^2 + y^2)$ for $F_{max} = 1.1 \times 10^5$ V/cm and a = 3.5 mm. The assumed velocity was 5×10^8 cm/sec

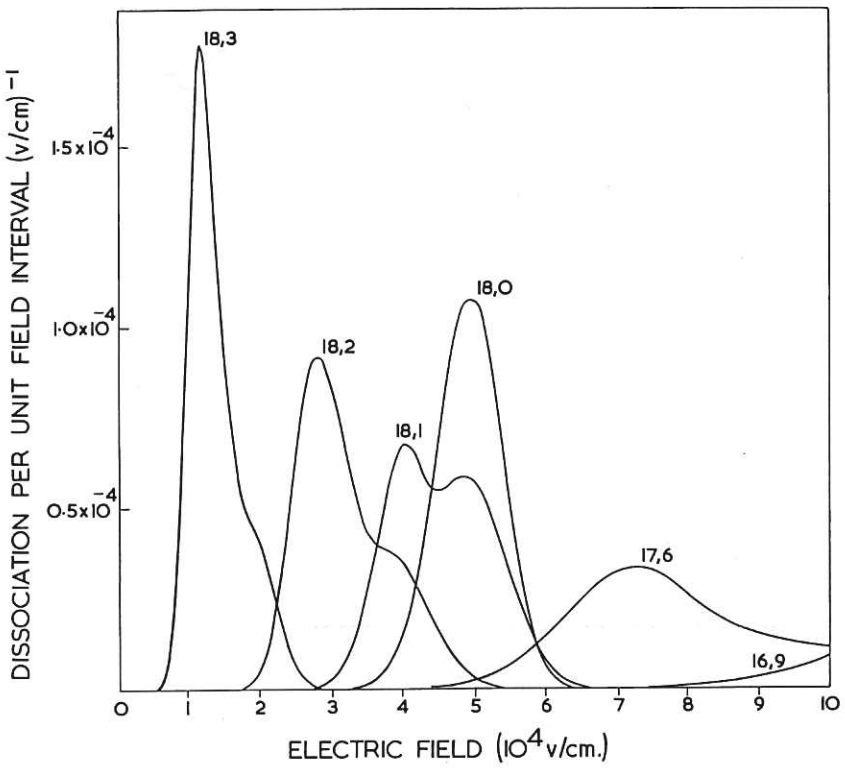

Fig. 32(b)
Dissociation probability when assuming an isotropic distribution among the various orientational quantum numbers; the integrated population is put to unity. The same field is assumed as in Fig. 31(a)

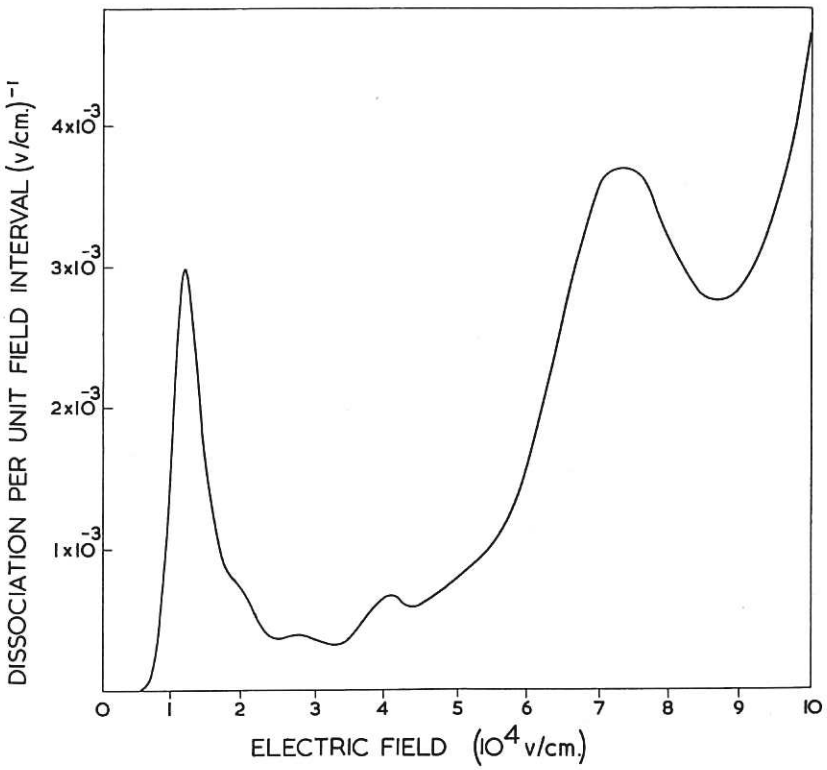

Fig. 32(c)
Dissociation probability when assuming a certain population of vibrational and rotational levels

Steps of $\Delta F = 0.05 \times 10^4$ V/cm were taken in the case of $v = 18$ and $\Delta F = 0.2 \times 10^4$ V/cm in the other cases.

The results are given in Fig.32(a). An initial population of unity was assumed in each case. We now assume an equal population among the m values. We then arrive at Fig.32(b) where we have assumed a population of unity for each vibrational rotational state. It can now be concluded that the first peak is due to $v = 18$, $J = 3$ and the second to $v = 17$, $J = 6$.

5.3 Estimation of the Populations

Having identified the observed peaks, we can now make an estimation of the population of the corresponding levels. We find that the level $v = 17$ $J = 6$ has a population about six times higher than $v = 18$ $J = 3$; whereas $v = 16$ $J = 9$ is about 10 times higher populated than $v = 18$ $J = 3$. The estimated errors are 25%. Fig.32c gives the theoretical curve for the estimated populations. The distribution among the various rotational levels in this model was chosen proportional to the statistical weight, which is $2J + 1$ for even values of J and three times this value for odd values of J. The reason for this is as follows

When we write the nuclear part of the wave function

$$\psi(\vec{r}_1, \vec{r}_2) = Y_{J,m}(\theta,\varphi)\ \Pi(r)$$

We note that interchanging $\vec{r}_1$ and $\vec{r}_2$ has the effect of changing θ by $\pi/2 - \theta$ hence changing the sign of $\cos\theta$. We now note that $P_J^m(x)$ is symmetric in x if J is even and antisymmetric of J is odd. Since

$$Y_{J,m}(\theta,\varphi) = C\ P_J^m(\cos\theta)e^{\,im\varphi}$$

we find that $\psi(\vec{r}_1, \vec{r}_2)$ is symmetric if J is even and antisymmetric if J is odd.

The protons being Fermions the nuclear part of the wave function must be symmetrical. This, however, does not exclude even J since for the total nuclear wave function the nuclear spin is to be taken into account. For protons this is $+\frac{1}{2}$. There are therefore for each proton two stationary states defined by $\chi_\alpha(\sigma)$ and $\chi_\beta(\sigma)$ which are defined by

$$\chi_\alpha(1) = 1 \qquad \chi_\beta(1) = 0$$

$$\chi_\alpha(-1) = 0 \qquad \chi_\beta(-1) = 1$$

A pair of protons will then have four stationary states, described by the wave functions

$$\chi_\alpha(\sigma_1)\ \chi_\alpha(\sigma_2)$$

$$\chi_\alpha(\sigma_1)\ \chi_\beta(\sigma_2) + \chi_\alpha(\sigma_2)\ \chi_\beta(\sigma_1)$$

$$\chi_\alpha(\sigma_1)\ \chi_\beta(\sigma_2) - \chi_\alpha(\sigma_2)\ \chi_\beta(\sigma_1)$$

$$\chi_\beta(\sigma_1)\ \chi_\beta(\sigma_2)$$

The suffixes 1,2 refer to the spin coordinates of the two particles.

It can be seen that three of these functions are symmetrical and one (the third) antisymmetrical. The complete wave function for the position and spin of the protons, which must be antisymmetric may have either of the two forms

$$\psi_S\ (r_1, r_2)\ \chi_A(\sigma_1, \sigma_2)$$

$$\psi_A\ (r_1, r_2)\ \chi_S(\sigma_1, \sigma_2)$$

where the suffix S denotes symmetrical and A antisymmetrical. The conclusion can now be drawn that odd values of J are three times as likely as even values of J.

When we now return to the experimental data and compare these with the theoretical ones we note that the absolute population of the $v = 18$ $J = 3$ level is 6×10^{-7}.

The 'half' peak at 2.6×10^4 V/cm, however, cannot be readily explained when assuming a reasonable population of the levels considered. A possible explanation may be the population of levels in the anti-bonding state $2p\sigma_u$.

Hiskes[26] estimated these levels to be populated in the same order of magnitude as the population of the $v = 18$ level when H_2^+ is formed from H_3^+.

The corresponding fields necessary for dissociation lie in the range 0.7×10^4 V/cm to 4.0×10^4 V/cm.

We can conclude that two of the observed peaks can be explained satisfactorily and moreover that there appears to be a measurable population of the anti-bonding state.

6. ACKNOWLEDGMENTS

The author is greatly indebted to Dr. A.C. Riviere and Dr. J.R. Hiskes for valuable discussions and to Culham Laboratory for the opportunity to carry out these investigations.

7. REFERENCES

1. POSTMA, H., HASTE, G.R. and DUNLAP, J.L. Proton trapping in DCX-1 from Lorentz dissociation of H_2^+. Nuclear Fusion, vol.3, no.2, June 1963. pp.128-129.

2. NIESSEN, K.F. Zur Quanten theorie des Wasserstoffmolekülions. (Thesis). Utrecht, 1922.

3. PAULI, W., jr. The model of the hydrogen molecule-ion. Ann. Physik, vol.68, 1922. pp.177-240.

4. SOMMERFELD, A. Atombau und Spektrallinien. 4 Auflage. Braunschweig, Fr. Vieweg und Sohn, 1924.

5. ALEXANDROW, W. Undulation mechanics of the molecular ion of hydrogen. Ann. Physik, vol.81, no.6, October 26, 1926. pp.577-586.

6. ALEXANDROW, W. Undulation mechanics of the molecular ion of hydrogen. Ann. Physik, vol.82, no.5, March 22, 1927. pp.683-688.

7. HUND, F. Zur deutung der Molekelspektren.I. Z. fur Physik, vol.40, no.10, 8 January 1927. pp.742-764.

8. BURRAU, Ø. Calculation of the energy value of the ionized hydrogen molecule in its normal state. Kgl. Danske Videnskab. Selskab, Math.-fys. Medd., vol.7, no.14, 1927.

9. HYLLERAAS, E.A. Uber die Elektronenterme des Wasserstoffmoleküls. Z. fur Physik, vol.71, nos.11/12, 26 September 1931. pp.739-763.

10. JAFFE, G. Zur Theorie des Wasserstoffmolekülions. Z. fur Physik, vol.87, nos.7/8, 26 January 1934. pp.535-544.

11. BATES, D.R., LEDSHAM, K. and STEWART, A.L. Wave functions of the hydrogen molecular ion. Phil. Trans. Roy. Soc., A, vol.246, no.911, November, 1953. pp.215-240.

12. COHEN, S., JUDD, D.L. and RIDDELL, R.J. Tabulation of potential functions and dynamic correction terms for the hydrogen molecular ion. Univ. of California, Lawrence Radiation Lab. Report no. UCRL-8802, June 1959.

13. COHEN, S., HISKES, J.R. and RIDDELL, R.J. Vibrational states of the hydrogen molecular ion. Phys. Rev., vol.119, no.3, August 1, 1960. pp.1025-1027.

14. RIVIERE, A.C. and SWEETMAN, D.R. Dissociation of H_2^+ and He^- by electric fields. Phys. Rev. Letters, vol.5, no.12, December 15, 1960. pp.560-562.

15. EHLER, A.W. Dissociation of vibrationally excited H_2^+ ions by an electric field. J. Appl. Phys., vol.35, no.10, October, 1964. pp.2858-2861.

16. KAPLAN, S., PAULIKAS, G.A. and PYLE, R.V. Dissociation of H_2^+ ions by a magnetic field. Phys. Rev. Letters, vol.7, no.3, August 1, 1961. pp.96-97.

17. BARNETT, C.F., RAY, J.A. and THOMPSON, J.C. Atomic and molecular collision cross sections of interest in controlled thermonuclear research. Oak Ridge National Laboratory Report no. ORNL-3113(rev), August, 1964. p.33.

18. RIVIERE, A.C. and SWEETMAN, D.R. The dissociation of molecular ions by strong electric fields. 5th Int. Conf. on Ionization Phenomena in Gases, Munich, 1961. Proceedings, Amsterdam, North Holland Pub. Co., 1962. pp.1236-1250.

19. BORN, M. and OPPENHEIMER, R. Quantum theory of the molecules. Ann. Physik, vol.84, 1927. pp.457-484.

20. MESSIAH, A. Quantum mechanics. vol.2. p.781. Amsterdam, North Holland Pub. Co., 1962.

21. WIND, H. Electron energy for H_2^+ in the ground state. J. Chem. Phys., vol.42, no.7, 1 April, 1965. pp.2371-2373.

22. BATES, D.R. ed. Quantum theory. Vol.1, Elements. New York, Academic Press, 1961. pp.122.

23. BETHE, H. Quantenmechanik der Ein-und Zwei-Elektronenprobleme. In: Geiger, H. and Scheel, K., eds. Handbuch der Physik, vol.24/1, p.527. Berlin, Springer-Verlag, 1933.

24. COHEN, S., JUDD, D.L. and RIDDELL, R.J. Mu-mesonic molecules. 1, Three-body problem. Phys. Rev., vol.119, no.1, July 1, 1960. pp.384-397.

25. KOPAL, Z. Numerical analysis. 2nd ed. London, Chapman & Hall, 1961. p.196.

26. HISKES, J.R. Electric and magnetic dissociation and ionization of molecular ions and neutral atoms. Nucl. Fusion, vol.2, nos.1/2, September 1962. pp.38-48.

27. HISKES, J.R. Dissociation of molecular ions by electric and magnetic fields. Phys. Rev., vol.122, no.4, May 15, 1961. pp.1207-1217.

28. WIND, H. Threshold electrical field for dissociation of the H_2^+ ion. Proc. Phys. Soc., vol.84, pt.4, October, 1964. pp.617-619.

29. COSSLETT, V.E. Introduction to electron optics. 2nd ed. Oxford, Clarendon Press, 1950. p.20.

30. RIVIERE, A.C. and SWEETMAN, D.R. Energy resolution of CsI (Tl) scintillation counter for 12.5 to 100 keV protons.

31. SWEETMAN, D.R. The dissociation of fast H_2^+ ions by hydrogen. Proc. Roy. Soc. A, vol.256, no.1286, 5 July 1960. pp.416-426, and Private communication.

32. RIVIERE, A.C. and SWEETMAN, D.R. A search for vibrational energy effects in the dissociation of H_2^+ ions by hydrogen gas. Proc. Phys. Soc., vol.78, no.505, 1 December 1961. pp.1215-1217.

33. HISKES, J.R. Dissociation of moecular ions by electric fields. University of California, Lawrence Radiation Laboratory, Report no. UCRL-9182, May 1960.

Available from

HER MAJESTY'S STATIONERY OFFICE

49 High Holborn, London, W.C.1
423 Oxford Street, London W.1
13a Castle Street, Edinburgh 2
109 St. Mary Street, Cardiff
Brazennose Street, Manchester 2
50 Fairfax Street, Bristol 1
35 Smallbrook, Ringway, Birmingham 5
80 Chichester Street, Belfast

or through any bookseller.

Printed in England

S.O. Code No. 91-3-18-41